A COMPREHENSIVE ANALYSIS OF UNCERTAINTIES AFFECTING THE STELLAR MASS – HALO MASS RELATION FOR 0 < z < 4

PETER S. BEHROOZI[1], CHARLIE CONROY[2], RISA H. WECHSLER[1]
Draft version May 12, 2010

ABSTRACT

We conduct a comprehensive analysis of the relationship between central galaxies and their host dark matter halos, as characterized by the stellar mass – halo mass (SM–HM) relation, with rigorous consideration of uncertainties. Our analysis focuses on results from the abundance matching technique, which assumes that every dark matter halo or subhalo above a specific mass threshold hosts one galaxy. We provide a robust estimate of the SM–HM relation for $0 < z < 1$ and discuss the quantitative effects of uncertainties in observed galaxy stellar mass functions (GSMFs) (including stellar mass estimates and counting uncertainties), halo mass functions (including cosmology and uncertainties from substructure), and the abundance matching technique used to link galaxies to halos (including scatter in this connection). Our analysis results in a robust estimate of the SM–HM relation and its evolution from z=0 to z=4. The shape and evolution are well constrained for $z < 1$. The largest uncertainties at these redshifts are due to stellar mass estimates (0.25 dex uncertainty in normalization); however, failure to account for scatter in stellar masses at fixed halo mass can lead to errors of similar magnitude in the SM–HM relation for central galaxies in massive halos. We also investigate the SM–HM relation to $z = 4$, although the shape of the relation at higher redshifts remains fairly unconstrained when uncertainties are taken into account. We find that the integrated star formation at a given halo mass peaks at 10-20% of available baryons for all redshifts from 0 to 4. This peak occurs at a halo mass of $7 \times 10^{11} M_\odot$ at $z = 0$ and this mass increases by a factor of 5 to $z = 4$. At lower and higher masses, star formation is substantially less efficient, with stellar mass scaling as $M_* \sim M_h^{2.3}$ at low masses and $M_* \sim M_h^{0.29}$ at high masses. The typical stellar mass for halos with mass less than $10^{12} M_\odot$ has increased by $0.3 - 0.45$ dex for halos since $z \sim 1$. These results will provide a powerful tool to inform galaxy evolution models.

Subject headings: dark matter — galaxies: abundances — galaxies: evolution — galaxies: stellar content — methods: N-body simulations

1. INTRODUCTION

A variety of physical processes are thought to be responsible for the observed distribution of galaxy properties, and distinguishing among them is one of the principal goals of modern galaxy formation theory. Among the relevant mechanisms are those responsible for galaxy growth, such as star formation and galaxy mergers, as well as those responsible for regulating growth, including energetic feedback by supernovae, active galactic nuclei, cosmic ray pressure, and long gas cooling times.

A fruitful approach to separating the influence of different mechanisms is to constrain the redshift–dependent relation between physical characteristics of galaxies, such as stellar mass, and the mass of their dark matter halos. This is possible because it is expected that many of these physical processes depend primarily on the mass of a galaxy's dark matter halo. By connecting galaxies to their parent halos, one is able to more clearly identify and constrain the physical processes responsible for galaxy growth.

The galaxy stellar mass – halo mass relation has additional utility because many properties of both galaxies and halos are tightly correlated with halo mass. In addition, the stellar mass – halo mass relation provides a mechanism for connecting predictions for the halo mass function and the mass–dependent spatial clustering of halos to the abundances and clustering of galaxies. If a model for galaxy evolution is able to reproduce the intrinsic galaxy mass – halo mass relation in the correct cosmological model, then such a model will match both the observed stellar mass function and the stellar mass dependent clustering of galaxies. Simultaneously matching these two observational quantities and their evolution has been difficult with either hydrodynamical simulations or semi-analytic models of galaxy formation (e.g., Weinberg et al. 2004; Li et al. 2007).

There are several ways to constrain the galaxy mass – halo mass relation. The first type of approach attempts to directly measure the mass of galactic halos. Techniques include weak lensing (e.g., Guzik & Seljak 2002; Sheldon et al. 2004; Mandelbaum et al. 2006) and the use of satellite galaxy or stellar velocities as tracers of the halo potential well (e.g., Ashman et al. 1993; Zaritsky & White 1994; Prada et al. 2003; van den Bosch et al. 2004; Conroy et al. 2007). While such methods are a relatively direct probe of halo mass, they are limited in dynamic range; current observations probe halo masses from roughly 10^{12}–$10^{14} M_\odot$ at the present epoch, and a smaller range at higher redshift. A second approach is to identify groups and clusters of galaxies either through optical or X-ray selected cluster catalogs, and then directly measure their galaxy content (e.g., Lin & Mohr 2004; Hansen et al. 2009; Yang et al. 2007). This is limited to relatively massive halos (although for optically identified groups it could extend to lower masses as new surveys probe dimmer galaxies in large enough volumes), and it also requires accurate knowledge of the mass–observable relation

[1] Kavli Institute for Particle Astrophysics and Cosmology; Physics Department, Stanford University, and SLAC National Accelerator Laboratory, Stanford, CA 94305
[2] Department of Astrophysical Sciences, Princeton University, Princeton, NJ 08544

(Yang et al. 2007; Hansen et al. 2009).

An alternative approach is to assume that the properties of the halo population are known, for example from cosmological simulations, and then find a functional form relating galaxies to halos which achieves agreement with a variety of observations. This approach is less direct but can be applied over a much larger dynamic range. Halo occupation (e.g., Berlind & Weinberg 2002; Bullock et al. 2002; Cooray & Sheth 2002; Tinker et al. 2005; Zheng et al. 2007) and conditional luminosity function modeling (e.g., Yang et al. 2003; Cooray 2006) fall into this category.

In the past decade, a number of studies have found that this latter approach can be greatly simplified using a technique called abundance matching. In its most basic form, the technique assigns the most massive (or the most luminous) galaxies to the most massive halos monotonically. The technique thus requires as input only the observed abundance of galaxies as a function of mass, namely the galaxy stellar mass function (alternatively the galaxy luminosity function) and the abundance of dark matter halos as a function of mass, namely the halo mass function. This technique has been shown to accurately reproduce a variety of observational results including various measures of the redshift– and scale–dependent spatial clustering of galaxies (Colín et al. 1999; Kravtsov & Klypin 1999; Neyrinck et al. 2004; Kravtsov et al. 2004; Vale & Ostriker 2004, 2006; Tasitsiomi et al. 2004; Conroy et al. 2006; Shankar et al. 2006; Berrier et al. 2006; Marín et al. 2008; Guo et al. 2009; Moster et al. 2009). In the context of this technique, not only central halos but also subhalos (halos contained within the virial radii of larger halos) are included in the matching process, meaning that satellite galaxies can be accounted for without any additional parameters.

Applications of the abundance matching technique have typically focused on using the default modeling assumptions to derive statistical information about the galaxy – halo connection. Uncertainties in the derived galaxy mass – halo mass relation have received little systematic attention in the context of this technique (though see Moster et al. 2009, for a recent treatment of the attendant uncertainties). An accurate assessment of the uncertainties is necessary to make strong statements regarding the underlying physical processes responsible for the derived galaxy – halo relation. In the present work we undertake an exhaustive exploration of the uncertainties relevant in constructing the galaxy stellar mass – halo mass relation from the abundance matching technique. We consider a range of uncertainties related to the observational stellar mass function, the theoretical halo mass function, and the underlying technique of abundance matching. The resulting galaxy stellar mass – halo mass relation and associated uncertainties will provide a benchmark against which galaxy evolution models may be fruitfully tested.

This paper is divided into several sections. In §2 we detail known sources of uncertainty which may affect our results. Our methodology for modeling the effects of uncertainties is discussed in §3, providing simple conversions where possible to allow for different modeling choices. We present our resulting estimates of the galaxy stellar mass – halo mass relation for $z < 1$ in §4 and describe the contribution of each of the uncertainties to the overall error budget. Estimates for the evolution of the relation out to $z \sim 4$, for which the uncertainties are significantly less well-understood, are presented in §5. Finally, we discuss the implications of this work in §6 and summarize our conclusions in §7.

Stellar masses throughout are quoted assuming a Chabrier (2003) initial mass function (IMF), the stellar population synthesis models of Bruzual & Charlot (2003), and the age and dust models in Blanton & Roweis (2007). We consider multiple cosmologies in this paper, but the main results assume a WMAP5+SN+BAO concordance ΛCDM cosmology (Komatsu et al. 2009) with $\Omega_M = 0.27$, $\Omega_\Lambda = 1 - \Omega_M$, $h = 0.7$, $\sigma_8 = 0.8$, and $n_s = 0.96$.

2. UNCERTAINTIES AFFECTING THE STELLAR MASS TO HALO MASS RELATION

Uncertainties in the abundance matching technique for assigning galaxies to dark matter halos can be conceptually separated into three classes. The first is uncertainty in the abundance of galaxies as a function of stellar mass. This class includes both uncertainties in counting galaxies due to shot noise and sample variance, as well as uncertainties in the stellar mass estimates themselves. The second class concerns the dark matter halos, and includes uncertainties in cosmological parameters, the impact of baryon condensation, and substructure. Finally, there are uncertainties in the process of matching galaxies to halos arising primarily from the intrinsic scatter between galaxy stellar mass and halo mass. Each of these sources of uncertainty are described in detail below. The detailed modeling of these uncertainties is described in §3.

2.1. *Uncertainties in the Stellar Mass Function*

Galaxy stellar masses are not measured directly, but are instead inferred from photometry and/or spectra. In particular, as the observed stellar light is a function of many physical processes (e.g., stellar evolution, star formation history and metal–enrichment history, and wavelength–dependent dust attenuation), stellar masses are estimated via complicated models to find the best fit to galaxy observations in a very large parameter space. Assumptions and simplifications in these models, along with the fact that the best fit may be only one of a number of likely possibilities, mean that there can be substantial uncertainties in calculated stellar masses.

Different types of observations can yield different uncertainties in these calculations. Spectroscopic surveys generally recover more spectral features per galaxy and more accurate redshifts than photometric surveys. However, spectroscopy requires substantially more telescope time than photometry. Therefore, spectroscopic samples tend to be limited both in area and depth, which translates into limitations in both volume and the minimum stellar mass probed. An additional problem for spectroscopic surveys such as the Sloan Digital Sky Survey (SDSS, York et al. 2000) is that the spectra probe only the central regions of galaxies (the SDSS spectra gather on average $1/3$ of the total flux from galaxies at $z = 0.1$). For galaxies containing both a bulge and a disk, or galaxies with radial gradients, the spectra will therefore not provide a fair sample of the entire galaxy (e.g., Kewley et al. 2005); furthermore, this bias will be a function of redshift. For these reasons, especially for robust comparisons of evolution, we confine this paper to photometric–based stellar masses; however, samples with spectroscopic redshifts are used where available.

2.1.1. *Principal Uncertainties in Stellar Mass Functions*

In this paper, we analyze seven main sources of uncertainties in stellar mass functions applicable to photometric surveys, listed below in rough order of importance.

1. *Choice of stellar initial mass function (IMF):* The luminosity of stars scales as their mass to a large power ($\mathrm{d}\ln L/\mathrm{d}\ln M \sim 3.5$), while the IMF, defined as the number of stars formed per unit mass, scales approximately as $\xi \propto M^{-2.3}$ (Salpeter 1955). Thus, the light from a galaxy is dominated by the most massive stars, while the total stellar mass is dominated by the lowest mass stars. This fact, which has been known for decades (e.g., Tinsley & Gunn 1976), implies that the assumed form of the IMF at $M \lesssim 0.5 M_\odot$ will have no effect on the integrated light from galaxies, but will have a large effect on the total stellar mass. Nonetheless, constraints on the total dynamical mass of spheroidal systems provide a valuable independent check on the form of the IMF at low masses. Cappellari et al. (2006) find, for example, that the IMF proposed by Chabrier (2003) for the Solar neighborhood is consistent with dynamical constraints on masses of nearby ellipticals.

   We do not marginalize over IMFs in our error calculations for the reason that it is relatively simple to convert from our choice of IMF (Chabrier 2003) to other IMFs. For our purposes the IMF becomes a serious source of systematic uncertainty only if the IMF varies with galaxy properties or if it evolves. It should be noted, however, that the IMF can also introduce more complicated systematic effects associated with the inferred star formation rate, which may in turn impact stellar masses in non–trivial ways (e.g. Conroy et al. 2010).

2. *Choice of Stellar Population Synthesis (SPS) model:* SPS modeling efforts have grown substantially in sophistication in the past decade (e.g. Leitherer et al. 1999; Bruzual & Charlot 2003; Le Borgne et al. 2004; Maraston 2005). Yet, significant uncertainties remain (e.g., Charlot et al. 1996; Charlot 1996; Yi 2003; Lee et al. 2007; Conroy et al. 2009). Treatments of convection vary, leading to different main sequence turn off times for intermediate mass stars. Advanced stages of stellar evolution, including blue stragglers, thermally–pulsating AGB stars (TP–AGB), and horizontal branch stars, are poorly understood, both observationally and theoretically. The theoretical spectral libraries contain known deficiencies, especially for M giants, where the effective temperatures are low and where hydrodynamic effects become important. Empirical stellar libraries to some extent circumvent these issues, although they are plagued by incomplete coverage in the HR diagram and difficulties associated with deriving stellar parameters. See Conroy et al. (2009) and Percival & Salaris (2009) for recent reviews.

   Different stellar population synthesis models treat these issues differently, which can result in large systematic differences in the derived stellar mass. For instance, the model of Maraston (2005) compared to Bruzual & Charlot (2003) has systematic differences of 0.1dex in stellar mass (Salimbeni et al. 2009; Pérez-González et al. 2008). However, Salimbeni et al. (2009) reports that the model in Bruzual (2007) (with a revised treatment of TP-AGB stars) yields systematic differences in stellar mass relative to Bruzual & Charlot (2003), which ranges from 0.05dex for $10^{11} M_\odot$ galaxies to 0.3dex for $10^{9.5} M_\odot$ galaxies. Conroy et al. (2009) show that uncertainty in the luminosity of the TP-AGB phase can shift stellar masses by as much as ± 0.2 dex.

3. *Parameterization of star formation histories:* In order to estimate stellar masses, model libraries are constructed with a large range in star formation histories (SFHs), dust attenuation (see below), and, often but not always, metallicity. The adopted functional form of the SFH is another source of systematic uncertainty, as typically very simple functional forms are assumed. Several authors have investigated various aspects of this problem. When attempting to model observed photometry, Pérez-González et al. (2008) found that a single stellar population model (in particular, star formation proportional to $e^{-t/\tau}$, which is a commonly-used parameterization) systematically underpredicts stellar mass by 0.18 dex compared to a double stellar population model (exponentially decaying star formation followed by a later starburst). The particular parameterization of SFHs may also lead to systematic differences as a function of stellar mass. Lee et al. (2009) analyzed a sample of mock Lyman–break galaxies at $z \sim 4-5$ and found that simple SFHs produced best–fit stellar masses that were under or overestimated by $\sim \pm 50\%$ depending on the rest-frame galaxy color. This bias was attributed to the chaotic SFHs of the mock galaxies.

4. *Choice of dust attenuation model:* Because dust reddens starlight, it is difficult to separate the effects of dust from stellar population effects, especially when fitting optical photometry. The effects of dust are also known to change depending on galaxy inclination (e.g., Driver et al. 2007). Hence, the choice of dust attenuation law has a nontrivial effect on the inferred stellar population ages and, consequently, star formation histories derived from photometric and even spectroscopic surveys (Panter et al. 2007). In terms of the effect on stellar masses, Pérez-González et al. (2008) compared the dust models of Calzetti et al. (2000) and Charlot & Fall (2000), finding a systematic difference of 0.10dex. Panter et al. (2007) found a similar difference between Calzetti et al. and models based on extinction curves from the Small and Large Magellanic Clouds. The effects of varying dust attenuation models have also been explored recently by Marchesini et al. (2009) and Muzzin et al. (2009), with similar results. We have used the stellar population fitting procedure described in Conroy et al. (2009) to compare the Calzetti et al. dust attenuation law to the dust model used in the `kcorrect` package (Blanton & Roweis 2007). We find a median offset of 0.02dex but also a systematic trend such that two galaxies whose stellar masses are estimated with Calzetti dust attenuation and are separated by 1.0dex will have `kcorrect` masses separated by (on average) only 0.92dex.

5. *Statistical errors in individual stellar mass estimates:* Stellar mass estimates for each galaxy are subject to statistical errors due to uncertainty in photometry as well as uncertainty in the SPS parameters for a given set of model assumptions. We treat this here as a random statistical error. While it may seem that random scatter in individual stellar masses should on average have no systematic effect, it in fact introduces a systematic error analogous to Eddington bias (Eddington

1940) observed in luminosity functions. As the stellar mass function drops off steeply beyond a certain characteristic stellar mass, there are many more low stellar mass galaxies that can be up-scattered than there are high stellar mass galaxies that can be down-scattered by errors in stellar mass estimates. This asymmetric scatter implies that the drop-off in number density at high masses becomes shallower in the presence of scatter. We discuss this effect in detail in §3.1.2 (see also the Appendix in Cattaneo et al. 2008).

6. *Sample variance:* Surveys of finite regions of the Universe are susceptible to large–scale fluctuations in the number density of galaxies. This is no longer a dominant source of uncertainty for the volumes probed at low redshift by the SDSS, but it is an important consideration for higher–redshift surveys, which cover much smaller comoving volumes. Most authors who consider sample variance attempt to minimize it by averaging over several fields (e.g., Pérez-González et al. 2008; Marchesini et al. 2009). Very few surveys at $z > 0$ attempt to estimate the magnitude of the error except by computing the field–to–field variance, which is often an underestimate when insufficient volume is probed (Crocce et al. 2009). We detail a more accurate method based on simulations to model the error arising from sample variance in §3.2.4.

7. *Redshift errors:* Photometric redshift errors blur the distinction between GSMFs at different redshifts. While a galaxy may be scattered either up or down in redshift space, volume-limited survey lightcones will contain larger numbers of galaxies at higher redshifts, meaning that the GSMF as reported at lower redshifts will be artificially inflated. Moreover, as galaxies at earlier times have lower stellar masses, surveys will tend to report artificially larger faint-end slopes in the GSMF. However, as these errors are well known, it is easy to correct for their effects on the stellar mass function, as has been done for the data in Pérez-González et al. (2008) (see the appendix of Pérez-González et al. 2005 for details on this process).

For completeness, we remark that galaxy-galaxy lensing will also result in systematic errors in the GSMF at high redshifts because galaxy magnification will result in higher observed luminosities. However, from ray-tracing studies of the Millennium simulation (Hilbert et al. 2007), the expected scatter in galaxy stellar masses from lensing is minimal (e.g., 0.04 dex at $z = 1$) compared to the other sources of scatter above (e.g., 0.25 dex from different model choices). For that reason, we do not model galaxy-galaxy lensing effects in this paper.

2.1.2. *Additional Systematics at $z > 1$*

Recently, it has become clear that current estimates of the evolution in the cosmic SFR density are not consistent with estimates of the evolution of the stellar mass density at $z > 1$ (Nagamine et al. 2006; Hopkins & Beacom 2006; Pérez-González et al. 2008; Wilkins et al. 2008a). The origin of this discrepancy is currently a matter of debate. One solution involves allowing for an evolving IMF with redshift (Davé 2008; Wilkins et al. 2008a). While such a solution is controversial, a number of independent lines of evidence suggest that the IMF was different at high redshift (Lucatello et al. 2005; Tumlinson 2007a,b; van Dokkum 2008). Reddy & Steidel (2009) offer a more mundane explanation for the discrepancy. They appeal to luminosity–dependent reddening corrections in the ultraviolet luminosity functions at high redshift, and demonstrate that the purported discrepancy then largely vanishes.

In contrast to results at $z > 1$, there does seem to be an accord that for $z < 1$ both the integrated SFR and the total stellar mass are in good agreement if one assumes (as we have) a Chabrier (2003) IMF (see Wilkins et al. 2008b; Pérez-González et al. 2008; Hopkins & Beacom 2006; Nagamine et al. 2006; Conroy & Wechsler 2009).

Because of the discrepancy between reported SFRs and stellar masses in the literature, it is clear that estimates of uncertainties in galaxy stellar mass functions and SFRs at $z > 1$ tend to underestimate the true uncertainties; for this reason, we separately analyze results for $z < 1$ in §4 and $z > 1$ in §5 of this paper.

2.2. *Uncertainties in the Halo Mass Function*

Dark matter halo properties over the mass range $10^{10} - 10^{15}$ $M_\odot$ have been extensively analyzed in simulations (e.g., Jenkins et al. 2001; Warren et al. 2006; Tinker et al. 2008), and the overall cosmology has been constrained by probes such as WMAP (Spergel et al. 2003; Komatsu et al. 2009). As such, uncertainties in the halo mass function have on the whole much less impact than uncertainties in the stellar mass function. We present our primary results for a fixed cosmology (WMAP5), but we also calculate the impact of uncertain cosmological parameters on our error bars. We do not marginalize over the mass function uncertainties for a given cosmology, as the relevant uncertainties are constrained at the 5% level (when baryonic effects are neglected, see below; Tinker et al. 2008). Additionally, in Appendix A, a simple method is described to convert our results to a different cosmology using an arbitrary mass function. For completeness, we mention the three most significant uncertainties here:

1. *Cosmological model:* The stellar mass – halo mass relation has dependence on cosmological parameters due to the resulting differences in halo number densities. We investigate this both by calculating the relation for two specific cosmological modes (WMAP1 and WMAP5 parameters) and then by calculating the uncertainties in the relation over the full range of cosmologies allowed by WMAP5 data. We find that in all cases these uncertainties are small compared to the uncertainties inherent in stellar mass modeling (§2.1.1), although they are larger than the statistical errors for typical halo masses at low redshift.

2. *Uncertainties in substructure identification:* Different simulations have different methods of identifying and assigning masses to substructure. Our matching methods make use only of the subhalo mass at the epoch of accretion (M_{acc}) as this results in a better match to clustering and pair–count results (Conroy et al. 2006; Berrier et al. 2006), so we are largely immune to the problem of different methods for calculating subhalo masses. Of greater concern is the ability to reliably follow subhalos in simulations as they are tidally stripped. Two related issues apply here. The first is that it is not clear how to account for subhalos which fall below the

resolution limit of the simulation. The second is that the formation of galaxies will dramatically increase the binding energy of the central regions of subhalos, potentially making them more resilient to tidal disruption. Hydrodynamic simulations suggest that this latter effect is small except for subhalos that orbit near the centers of the most massive clusters (Weinberg et al. 2008). However, while these details are important for accurately predicting the clustering strength on small scales ($\lesssim 1$ Mpc), they are not a substantial source of uncertainty for the global halo mass — stellar mass relation because satellites are always sub-dominant ($\lesssim 20\%$) by number. We discuss the analytic method we use to model the satellite contribution to the halo mass function in §3.2.2.

3. *Baryonic physics:* Recent work by Stanek et al. (2009) suggests that gas physics can affect halo masses relative to dark matter-only simulations by -16% to +17%, leading to number density shifts of up to 30% in the halo mass function at $10^{14} M_\odot$. Without evidence for a clear bias in one direction or the other—the models of gas physics still remain too uncertain—we do not apply a correction for this effect in our mass functions. Uncertainties of this magnitude are larger than the statistical errors in individual stellar masses at low redshift, but are still small in comparison to systematic errors in calculating stellar masses.

For completeness, we note that the effects of sample variance on halo mass functions estimated from simulations are small. Current simulations readily probe volumes of 1000 (h^{-1} Mpc)^3 (Tinker et al. 2008), and so the effects of sample variance on the halo mass function are dwarfed by the effects of sample variance on the stellar mass function; we therefore do not analyze them separately in this paper. We also remark on the issue of mass definitions. Although abundance matching implies matching the most massive galaxies to the most massive halos, there is little consensus on *which* halo mass definition to use, with popular choices being M_{vir} (mass within the virial radius), M_{200} (mass within a sphere with mean density $200\rho_{\rm crit}$), and M_{fof} (mass determined by a friends-of-friends particle linking algorithm). We choose M_{vir} for this paper and note that the largest effect of choosing another mass algorithm will be a purely definitional shift in halo masses. We expect that scatter between any two of these mass definitions is degenerate with and smaller than the amount of scatter in stellar masses at fixed halo mass (the latter effect is discussed in §2.3).

2.3. *Uncertainties in Abundance Matching*

Finally, there are two primary uncertainties concerning the abundance matching technique itself:

1. *Nonzero scatter in assigning galaxies to halos:* While host halo mass is strongly correlated with stellar mass, the correlation is not perfect. At a given halo mass, the halo merger history, angular momentum properties, and cooling and feedback processes can induce scatter between halo mass and galaxy stellar mass. This is expected to result in scatter in stellar of $\sim$0.1–0.2 dex at a given halo mass, see §3.3.1 for discussion. The scatter between halo mass and stellar mass will have systematic effects on the mean relation for reasons analogous

to those mentioned for statistical error in stellar mass measurements. At the high mass end where both the halo and stellar mass functions are exponential, scatter in stellar mass at fixed halo mass (or vice versa) will alter the average relation because there are more low mass galaxies that are upscattered than high mass galaxies that are downscattered.

2. *Uncertainty in Assigning Galaxies to Satellite Halos:* It is not clear that the halo mass — stellar mass relation should be the same for satellite and central galaxies. Once a halo is accreted onto a larger halo, it starts to lose halo mass because of dynamical effects such as tidal stripping. While stripping of the halo appears to be a relatively dramatic process (e.g., Kravtsov et al. 2004), the stripping of the stellar component probably does not occur unless the satellite passes very near to the central object because the stellar component is much more tightly bound than the halo. It is clear from the observed color–density relation (Dressler 1980; Postman & Geller 1984; Hansen et al. 2009) that star formation in satellite galaxies must eventually cease with respect to galaxies in the field. It is less clear how quickly star formation ceases, and whether or not there is a burst of star formation upon accretion. All of these issues can potentially alter the relation between halo and stellar mass for satellites (although the modeling results of Wang et al. 2006 suggest that the halo–satellite relation is indistinguishable from the overall galaxy–halo relation).

3. METHODOLOGY

Our primary goal is to provide a robust estimate of the stellar mass – halo mass relation over a significant fraction of cosmic time via the abundance matching technique. We aim to construct this relation by taking into account all of the relevant sources of uncertainty. This section describes in detail a number of aspects of our methodology, including our approach for incorporating uncertainties in the stellar mass function (§3.1), a summary of the adopted halo mass functions and associated uncertainties (§3.2), the uncertainties associated with abundance matching (§3.3), our choice of functional form for the stellar mass – halo mass relation, including a discussion of why certain functions should be preferred over others (§3.4), and the Markov Chain Monte Carlo parameter estimation technique (§3.5). For readers interested in the general outline of our process but not the details, we conclude with a brief summary of our methodology (§3.6).

3.1. *Modeling Stellar Mass Function Uncertainties*

As discussed in §2, there are several classes of uncertainties affecting the way the stellar mass function is used in the abundance matching process. In this section, we discuss systematic shifts in stellar mass estimates and the effects of statistical errors on the stellar mass function.

3.1.1. *Modeling Systematic Shifts in Stellar Mass Estimates*

Most studies on the GSMF report Schechter function fits as well as individual data points; many also provide statistical errors. However, even when systematic errors are reported (either in Schechter parameters or at individual data points), the systematic error estimates are of limited value unless one is also able to model shifts in the GSMF caused by such errors.

Fortunately, based on the discussion in §2.1.1, there seem to be two main classes of systematic errors causing shifts in the GSMF:

1. Over/underestimation of all stellar masses by a constant factor μ. This appears to cover the majority of errors, including most differences in SPS modeling, dust attenuation assumptions, and stellar population age models.

2. Over/underestimation of stellar masses by a factor which depends linearly on the logarithm of the stellar mass (i.e., depends on a power of the stellar mass). This covers the majority of the remaining discrepancies between different SPS models and different stellar age models.

Both forms of error are modeled with the equation

$$\log_{10}\left(\frac{M_{*,\mathrm{meas}}}{M_{*,\mathrm{true}}}\right) = \mu + \kappa \log_{10}\left(\frac{M_{*,\mathrm{true}}}{M_0}\right). \quad (1)$$

Without loss of generality, we may take $M_0 = 10^{11.3} M_\odot$ (the fixed point of the variation between the Bruzual 2007 and Bruzual & Charlot 2003 models found by Salimbeni et al. 2009), allowing the prior on M_0 to be absorbed into the prior on μ.

For the prior on μ, we consider four contributing sources of uncertainty. We adopt estimates of the uncertainty from the SPS model ($\approx$0.1dex), the dust model ($\approx$0.1dex), and assumptions about the star formation history ($\approx$0.2dex) from Pérez-González et al. (2008) as detailed in §2.1.1. Additionally, we have the variation in $\kappa \log_{10}(M_0)$ (at most 0.1dex, as $|\kappa| \lesssim 0.15$ — see below). Assuming that these are statistically independent, they combine to give a total uncertainty of 0.25dex, which is consistent with the accepted range for systematic uncertainties in stellar mass (Pérez-González et al. 2008; Kannappan & Gawiser 2007; van der Wel et al. 2006; Marchesini et al. 2009). For lack of adequate information (i.e., different models) to infer a more complicated distribution, we assume that μ has a Gaussian prior. As more studies of the overall systematic shift μ become available, our assumptions for the prior on μ and the probability distribution will likely need corrections. We remark, however, that our results can easily be converted to a different assumption for μ, as μ simply imparts a uniform shift in the intrinsic stellar masses relative to the observed stellar masses.

For the prior on κ, the result of Salimbeni et al. (2009) would suggest $|\kappa| \lesssim 0.15$. As mentioned in §2.1.1, we found that $|\kappa| \approx 0.08$ between the Blanton & Roweis (2007) and Calzetti et al. (2000) models for dust attenuation. Li & White (2009) finds $|\kappa| \lesssim 0.10$ between Blanton & Roweis (2007) and Bell et al. (2003) stellar masses. Without a large number of other comparisons, it is difficult to robustly determine the prior distribution for κ; however, motivated by the results just mentioned, we assume that the prior on κ is a Gaussian of width 0.10 centered at 0.0.

We remark that some authors have considered much more complicated parameterizations of the systematic error. For example, Li & White (2009) considers a four-parameter hyperbolic tangent fit to differences in the GSMF caused by different SPS models, as well as a five-parameter quartic fit. However, we do not consider higher-order models for systematic errors for several reasons. First, given that second- and higher-order corrections will result only in very small corrections to the stellar masses in comparison to the zeroth-order correction ($\mu \approx 0.25$dex), the corrections will not substantially effect the systematic error bars. Second, we do not know of any studies which would allow us to construct priors on the higher-order corrections. Finally, with higher-order models, there is the serious danger of over-fitting—that is, with very loose priors on systematic errors, the best-fit parameters for the systematic errors will be influenced by bumps and wiggles in the stellar mass function due to statistical and sample variance errors. Hence, the interpretive value of the systematic errors becomes increasingly dubious with each additional parameter.

3.1.2. *Modeling Statistical Errors in Individual Stellar Mass Measurements*

In addition to the systematic effects discussed in the previous section, measurement of stellar masses is subject to statistical errors. Even for a fixed set of assumptions about the dust model, SPS model, and the parameterization of star formation histories, stellar masses will carry uncertainties because the mapping between observables and stellar masses is not one-to-one. This additional source of uncertainty has unique effects on the GSMF. Observers will see an GSMF (ϕ_{meas}) which is the true or "intrinsic" GSMF (ϕ_{true}) convolved with the probability distribution function of the measurement scatter. For instance, if the scatter is uniform across stellar masses and has the shape of a certain probability distribution P, we have:

$$\phi_{\mathrm{meas}}(M) = \int_{-\infty}^{\infty} \phi_{\mathrm{true}}(10^y) P\left(y - \log_{10}(M)\right) dy, \quad (2)$$

where y is the integration variable, in units of $\log_{10}$ mass. As derived in Appendix B, the approximate effect of the convolution is

$$\log_{10}\left(\frac{\phi_{\mathrm{meas}}(M)}{\phi_{\mathrm{true}}(M)}\right) \approx \frac{\sigma^2}{2}\ln(10)\left(\frac{d\log\phi_{\mathrm{true}}(M)}{d\log M}\right)^2, \quad (3)$$

where σ is the standard deviation of P. That is to say, the effect of the convolution depends strongly on the logarithmic slope of ϕ_{true}. Where the slope is small (i.e., for low-mass galaxies), there is almost no effect. Above $10^{11} M_\odot$, where the GSMF becomes exponential, there can be a dramatic effect, with the result that ϕ_{true} is more than an order of magnitude less than ϕ_{meas} because it becomes far more likely that stellar mass calculation errors produce a galaxy of very high perceived stellar mass than it is for there to be such a galaxy in reality (see for example Cattaneo et al. 2008).

For the observed $z \sim 0$ GSMF, we take the probability distribution P to be log-normal with 1σ width 0.07dex from the analysis of the photometry of low–redshift luminous red galaxies (LRGs) (Conroy et al. 2009). Kauffmann et al. (2003) found similar results regarding the width of P. This function only accounts for the statistical uncertainties mentioned above and does not include additional systematic uncertainties. In light of Equation 3, we use LRGs to estimate P because LRGs occupy the high stellar mass regime where measurement errors are most likely to affect the shape of the observed GSMF. However, the single most important attribute of the distribution P is its width; the main results do not change substantially if an alternate distribution with non-Gaussian tails beyond the 1σ limits of P is used.

For higher redshifts, we scale the width of the probability distribution to account for the fact that mass estimates become less certain at higher redshift (e.g., Conroy et al. 2009;

Kajisawa et al. 2009):

$$P(\Delta \log_{10} M_*, z) = \frac{\sigma_0}{\sigma(z)} P_0 \left(\frac{\sigma_0}{\sigma(z)} \Delta \log_{10} M_* \right), \quad (4)$$

where P_0 is the probability distribution at $z = 0$ (as discussed above), σ_0 is the standard deviation of P_0, and $\sigma(z)$ gives the evolution of the standard deviation as a function of redshift.

Conroy et al. (2009) did not give a functional form for $\sigma(z)$, but they calculate for a handful of massive galaxies that $\sigma(z = 2)$ is ≈ 0.18dex, as compared to $\sigma(z = 0) \approx 0.07$dex. Kajisawa et al. (2009) performed a similar calculation (albeit with a different SPS model) of the distribution in several redshift bins; their results show gradual evolution for $\sigma(z)$ out to $z = 3.5$ for high stellar mass galaxies consistent with a linear fit:

$$\sigma(z) = \sigma_0 + \sigma_z z. \quad (5)$$

The results of Kajisawa et al. (2009) suggest that $\sigma_z = 0.03$-0.06 dex for LRGs. As this is consistent with the value of $\sigma_z = 0.05$ dex which would correspond to Conroy et al. (2009), we adopt the linear scaling of Equation 5 with a Gaussian prior of $\sigma_z = 0.05 \pm 0.015$ dex.

Note that the effect of this statistical error on the stellar mass function is minimal below $10^{11} \ M_\odot$, and therefore does not affect the stellar mass – halo mass relation for halos below $\sim 10^{13} \ M_\odot$, as discussed in §4.2. While this scatter does have an effect on the shape of the stellar mass function for high-mass galaxies, the qualitative predictions we make from this analysis are generic to all types of random scatter.

3.2. Halo Mass Functions

The halo mass function specifies the abundance of halos as a function of mass and redshift. A number of analytic models and simulation–based fitting functions have been presented for computing mass functions given an input cosmology (e.g., Press & Schechter 1974; Jenkins et al. 2001; Warren et al. 2006; Tinker et al. 2008). For most of our results we will adopt the universal mass function of Tinker et al. (2008), as described below. Analytic mass functions are preferable as they 1) allow mass functions to be computed for a range of cosmologies and 2) do not suffer significantly from sample variance uncertainties, because the analytic relations are typically calibrated with very large or multiple N–body simulations.

For some purposes it will be useful to also consider full halo merger trees derived directly from N–body simulations that have sufficient resolution to follow halo substructures. The simulations used herein will be described below, in addition to our methods for modeling uncertainties in the underlying mass function, including cosmology uncertainties, sample variance in the galaxy surveys, and our models for satellite treatment.

3.2.1. Simulations

For the principal simulation in this study ("L80G"), we used a pure dark matter N-body simulation based on Adaptive Refinement Tree (ART) code (Kravtsov et al. 1997; Kravtsov & Klypin 1999). The simulation assumed flat, concordance ΛCDM ($\Omega_M = 0.3$, $\Omega_\Lambda = 0.7$, $h = 0.7$, and $\sigma_8 = 0.9$) and included 512^3 particles in a cubic box with periodic boundary conditions and comoving side length $80h^{-1}$Mpc. These parameters correspond to a particle mass resolution of

$\approx 3.2 \times 10^8 h^{-1} M_\odot$. For this simulation, the ART code begins with a spatial grid size of 512^3; it refines the grid up to eight times in locally dense regions, leading to an adaptive distance resolution of $\approx 1.2 h^{-1}$kpc (comoving units) in the densest parts and $\approx 0.31 h^{-1}$Mpc in the sparsest parts of the simulation.

In this simulation, halos and subhalos were identified using a variant of the Bound Density Maxima algorithm (Klypin et al. 1999). Halo centers are located at peaks in the density field smoothed over a 24-particle SPH kernel (for a minimum resolvable halo mass of $7.7 \times 10^9 h^{-1} \ M_\odot$). Nearby particles are classified as bound or unbound in an iterative process; once all the locally bound particles have been found, halo parameters such as the virial mass $M_{\rm vir}$ and maximum circular velocity $V_{\rm max}$ may be calculated. (See Kravtsov et al. 2004 for complete details on the algorithm). The simulation is complete down to $V_{\rm max} \approx 100$ km s^{-1}, corresponding to a galaxy stellar mass of $10^{8.75} \ M_\odot$ at $z = 0$.

The ability of L80G to track satellites with high mass and force resolution gives it several uses. Merger trees from L80G inform our prescription for converting analytical central-only halo mass functions to mass functions which include satellite halos (see §3.2.2). Additionally, the merger trees allow for evaluation of different models of satellite stellar evolution with full consistency (see §3.3.2). Finally, the knowledge of which satellite halos are associated with which central halos allows for estimates of the total stellar mass (in the central and all satellite galaxies) — halo mass relation (see §4.3.6).

We also make use of a secondary simulation from the Large Suite of Dark Matter Simulations (LasDamas Project, http://lss.phy.vanderbilt.edu/lasdamas/) in our sample variance calculations. The L80G simulation is too small for use in calculating the sample variance between multiple independent mock surveys, but the larger size of the LasDamas simulation ($420 \ h^{-1}$ Mpc, 1400^3 particles) makes it ideal for this purpose. However, the LasDamas simulation has poorer mass resolution (a minimum particle size of $1.9 \times 10^9 \ M_\odot$) and force resolution ($8 \ h^{-1}$ kpc), making it unable to resolve subhalos (particularly after accretion) as well as L80G. The LasDamas simulation assumes a flat, ΛCDM cosmology ($\Omega_M = 0.25$, $\Omega_\Lambda = 0.75$, $h = 0.7$, and $\sigma_8 = 0.8$) which is very close to the WMAP5 best-fit cosmology (Komatsu et al. 2009). Collisionless gravitational evolution was provided by the GADGET-2 code (Springel 2005). Halos are identified using friends of friends with a linking length of 0.164. The subfind algorithm Springel (2005) is used to identify substructure.

As mentioned, the primary use of the LasDamas simulation is in sampling the halo mass functions in mock surveys to model the effects of sample variance on high-redshift pencil-beam galaxy surveys. The mock surveys are constructed so as to mimic the observations in Pérez-González et al. (2008). In each mock survey, three pencil-beam lightcones (matching the angular sizes of the three fields in Pérez-González et al. 2008) with random orientations are sampled from a random origin in the simulation volume out to $z = 1.3$. Thus, by comparing the halo mass functions in individual mock surveys to the mass function of the ensemble, the effects of sample variance may be calculated with full consideration of the correlations between halo counts at different masses.

3.2.2. Analytic Mass Functions

The analytic mass functions of Tinker et al. (2008) are used to calculate the abundance of halos in several cosmological
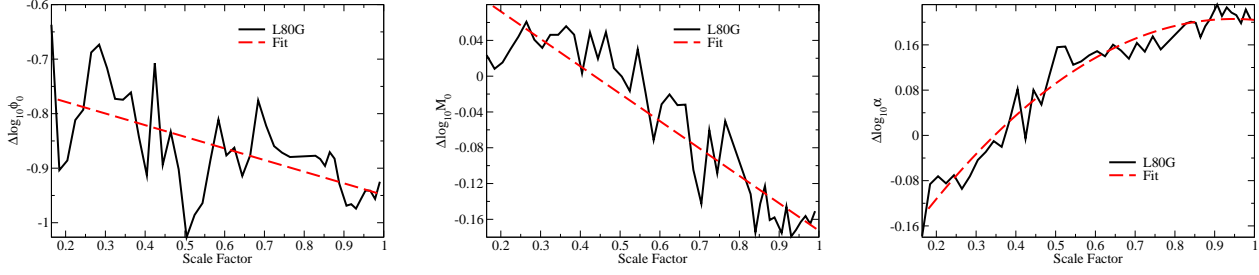
Figure 1. Differences between the fitted Schechter function parameters for the satellite halo mass (at accretion) function and the central halo mass function, as a function of scale factor; e.g., $\Delta \log_{10} \phi_0$ corresponds to $\log_{10}(\phi_{0,\text{sats}}/\phi_{0,\text{centrals}})$. The black lines are calculated from a simulation using WMAP1 cosmology (L80G), and the red lines represent the fits to the simulation results in Equation 7.

models. We calculate mass functions defined by M_{vir}, using the overdensity specified by Bryan & Norman (1998) [3] This results in an overdensity (compared to the mean background density) Δ_{vir} which ranges from 337 at $z = 0$ to 203 at $z = 1$ and smoothly approaches 180 at very high redshifts. Following Tinker et al. (2008), we use spline interpolation to calculate mass functions for overdensities between the discrete intervals presented in their paper.

The mass functions in Tinker et al. (2008) only include central halos. We model the small ($\approx 20\%$ at $z = 0$) correction to the mass function introduced by subhalos to first order only, as the overall uncertainty in the central halo mass function is already of order 5% (Tinker et al. 2008). In particular, we calculate satellite (mass at accretion) and central mass functions in our simulation (L80G) and fit Schechter functions to both, excluding halos below our completeness limit ($10^{10.3}\ M_\odot$). Then, we plot the difference between the Schechter parameters (the difference in characteristic mass, $\Delta \log_{10} M_*$; the difference in characteristic density, $\Delta \log_{10} \phi_0$; and the difference in faint-end slopes, $\Delta \alpha$) as a function of scale factor (a). This gives the satellite mass function (ϕ_s) as a function of the central mass function (ϕ_c), which allows us to use this (first-order) correction for central mass functions of different cosmologies:

$$\phi_s(M) = 10^{\Delta \log_{10} \phi_0} \left(\frac{M}{M_0 \cdot 10^{\Delta \log_{10} M_0}} \right)^{-\Delta \alpha} \phi_c(M/10^{\Delta \log_{10} M_0}).$$
(6)

From our simulation, we find fits as shown in Figure 1:[4]

$$\Delta \log_{10} \phi_0(a) = -0.736 - 0.213\,a,$$
$$\Delta \log_{10} M_0(a) = 0.134 - 0.306\,a,$$
(7)
$$\Delta \alpha(a) = -0.306 + 1.08\,a - 0.570\,a^2.$$

The mass function used here may be be easily replaced by an arbitrary mass function, as detailed in Appendix A.

3.2.3. *Modeling Uncertainties in Cosmological Parameters*

Our fiducial results are calculated assuming WMAP5 cosmological parameters. In order to model uncertainties in cosmological parameters, we have sampled an additional 100 sets of cosmological parameters from the WMAP5+BAO+SN

MCMC chains (from the models in Komatsu et al. 2009) and generated mass functions for each one according to the method in the previous section. Hence, to determine the variance in the derived stellar mass – halo mass relation caused by cosmology uncertainties, we recalculate the relation for each sampled mass function according to the method described in Appendix A.

3.2.4. *Estimating Sample Variance Effects for the Stellar Mass Function*

Large–scale modes in the matter power spectrum imply that finite surveys will obtain a biased estimate of the number densities of galaxies and halos as compared to the full universe. That is to say, matching observed GSMFs measured from a finite survey to the halo mass function estimated from a much larger volume will introduce systematic errors into the resulting SM–HM relation. These errors cannot be corrected unless one has knowledge of the halo mass function for the specific survey in question, which is in general not possible.

However, we can still calculate the uncertainties introduced by the limited sample size. While we cannot determine the true halo mass function for the survey, we can calculate the probability distribution of halo mass functions for identically shaped surveys via sampling lightcones from simulations. If we rematch galaxy abundances from the observed GSMF to the abundances of halos in each of the sampled lightcones, then the uncertainty introduced by sample variance is exactly captured in the variance of the resulting SM–HM relations.

In detail, we create our distribution of halo mass functions by sampling one thousand mock surveys from the Las-Damas simulation (see §3.2.1) corresponding to the exact survey parameters used in Pérez-González et al. (2008). We fit Schechter functions to the halo mass functions of each mock survey (over all redshifts), and we calculate the change in Schechter parameters ($\Delta \log_{10} \phi_0$, $\Delta \log_{10} M_0$, and $\Delta \alpha$) as compared to a Schechter fit to the ensemble average of the mass functions. Using the distribution of the changes in Schechter parameters, we may mimic to first order the expected distribution of halo mass functions for any cosmology. In particular, we use an equation exactly analogous to Equation 6 to convert the mass function for the full universe (ϕ_{full}) and the distribution of $\Delta \log_{10} \phi_0$, $\Delta \log_{10} M_0$, and $\Delta \alpha$ into a distribution of possible survey mass functions (ϕ_{obs}):

$$\phi_{\text{obs}}(M) = 10^{\Delta \log_{10} \phi_0} \left(\frac{M}{M_0 \cdot 10^{\Delta \log_{10} M_0}} \right)^{-\Delta \alpha} \phi_{\text{full}}(M/10^{\Delta \log_{10} M_0}).$$
(8)

Hence, to obtain the variance in the stellar mass – halo mass

---

[3] $\Delta_{\text{vir}} = (18\pi^2 + 82x - 39x^2)/(1+x); x = (1 + \rho_\Lambda(z)/\rho_M(z))^{-1} - 1$
[4] Comparing these fits to satellite mass functions from a more recent simulation (Klypin et al. 2010, the "Bolshoi" simulation), we have verified that applying these fits to mass functions for the WMAP5 cosmology introduces errors only on the level of 5% in overall number density, similar to the uncertainty with which the mass function is known.

relation caused by finite survey size, we recalculate the relation for each one of the survey mass functions thus computed according to the method described in Appendix A.

3.3. *Uncertainties in Abundance Matching*
3.3.1. *Scatter in Stellar Mass at Fixed Halo Mass*

An important uncertainty in the abundance matching procedure is introduced by intrinsic scatter in stellar mass at a given halo mass. Suppose that $M_*(M_h)$ is the average (true) galaxy stellar mass as a function of host halo mass. For a perfect monotonic correlation between stellar mass and halo mass, i.e., without scatter between stellar and halo mass, it is straightforward to relate the true or "intrinsic" stellar mass function (ϕ_{true}) to the halo mass function (ϕ_h) via

$$\frac{dN}{d\log_{10} M_*} = \frac{dN}{d\log_{10} M_h}\frac{d\log M_h}{d\log M_*}, \quad (9)$$

where N is the number density of galaxies, so that

$$\phi_{\text{true}}(M_*(M_h)) = \phi_h(M_h)\left(\frac{d\log M_*(M_h)}{d\log M_h}\right)^{-1}. \quad (10)$$

Intuitively, as the halos of mass M_h get assigned stellar masses of $M_*(M_h)$, the number density of galaxies with mass $M_*(M_h)$ will be proportional to the number density of halos with mass M_h. The above equations are simply a mathematical representation of the traditional abundance matching technique.

Equation 10 remains useful in the presence of scatter. If we know the expected scatter about the mean stellar mass, say in the form of a probability density function $P_s(\Delta \log_{10} M_* | M_h)$, then we may still relate ϕ_{true} to ϕ_h via an integral similar to a convolution:

$$\phi_{\text{true}}(x) = \int_0^\infty \phi_h(M_h(M_*))\frac{d\log M_h(M_*)}{d\log M_*} \times$$
$$\times P_s(\log_{10}\frac{x}{M_*}|M_h(M_*))d\log_{10} M_*, \quad (11)$$

where $M_h(M_*)$ is the inverse function of $M_*(M_h)$.

This similarity to a convolution is no coincidence—mathematically, it is analogous to how we model random statistical errors in stellar mass measurements in §3.1.2. Namely, if we define ϕ_{direct} to equal the right-hand side of Equation 10,

$$\phi_{\text{direct}}(M_*) \equiv \phi_h(M_h(M_*))\frac{d\log M_h}{d\log M_*}, \quad (12)$$

and if we assume a probability density distribution independent of halo mass (i.e., scatter in stellar mass at fixed halo mass is independent of halo mass), then ϕ_{true} is exactly related to ϕ_{direct} by a convolution:

$$\phi_{\text{true}}(M_*) = \int_{-\infty}^\infty \phi_{\text{direct}}(10^y)P_s(y - \log_{10} M_*)dy, \quad (13)$$

which is mathematically identical to Equation 2 in §3.1.2.

Then, if one calculates ϕ_{direct} from ϕ_{true}, one may find $M_h(M_*)$ via direct abundance matching. Namely, integrating equation 12, we have:

$$\int_{M_h(M_*)}^\infty \phi_h(M)d\log_{10} M = \int_{M_*}^\infty \phi_{\text{direct}}(M_*)d\log_{10} M_*. \quad (14)$$

Equivalently, letting $\Phi_h(M_h) \equiv \int_{M_h}^\infty \phi_h(M)d\log_{10} M$ be the cumulative halo mass function, and letting $\Phi_{\text{direct}}(M_*) \equiv$ $\int_{M_*}^\infty \phi_{\text{direct}}(M_*)d\log_{10} M_*$ be the cumulative "direct" stellar mass function, we have

$$M_h(M_*) = \Phi_h^{-1}(\Phi_{\text{direct}}(M_*)), \quad (15)$$

and one may similarly find $M_*(M_h)$ by inverting this relation.

Our approach in all equations except for Equation 13 allows a halo mass-dependent scatter in the stellar mass, but to date the data appears to be consistent with a constant scatter value. For example, using the kinematics of satellite galaxies, More et al. (2009) finds that the scatter in galaxy luminosity at a given halo mass is 0.16 ± 0.04 dex, independent of halo mass. Using a catalog of galaxy groups, Yang et al. (2009b) find a value of 0.17 dex for the scatter in the stellar mass at a given halo mass, also independent of halo mass. Here, we thus assume a fixed value for the scatter in stellar mass at fixed halo mass, ξ, to specify the standard deviation of $P_s(\Delta \log_{10} M_*)$. As the Yang et al. (2009b) value is consistent with the More et al. (2009) value, we set the prior using the More et al. (2009) value and error bounds on ξ, We assume a Gaussian prior on the probability distribution for ξ, and we assume that the scatter itself is log-normal.

3.3.2. *The Treatment of Satellites*

When a galaxy is accreted into a larger system, it will likely be stripped of dark matter much more rapidly than stellar mass because the stars are much more tightly bound than the halo. It has been demonstrated that various galaxy clustering properties compare favorably to samples of halos where satellite halos — i.e., subhalos — are selected according to their halo mass at the epoch of accretion, M_{acc}, rather than their current mass (e.g., Nagai & Kravtsov 2005; Conroy et al. 2006; Vale & Ostriker 2006; Berrier et al. 2006). These results support the idea that satellite systems lose dark matter more rapidly than stellar mass.

As commonly implemented (e.g. Conroy et al. 2006), the abundance matching technique matches the stellar mass function at a particular epoch to the halo mass function at the same epoch, using M_{acc} rather than the present mass for subhalos. As M_{acc} remains fixed as long as the satellite is resolvable, the standard technique implies that the satellite galaxy's stellar mass will continue to evolve in the same way as for centrals of that halo mass. Therefore, a subtle implication of the standard technique is that satellites may continue to grow in stellar mass, even though M_{acc} remains the same. A different model for satellite stellar evolution (e.g., in which stellar mass which does not evolve after accretion) would therefore involve different choices in the satellite matching process.

The fiducial results presented here use the standard model where satellites are assigned stellar masses based on the current stellar mass function and their accretion–epoch masses. However, we also present results for comparison in which satellite masses are assigned utilizing the stellar mass function at the epoch of accretion, corresponding to a situation in which satellite stellar masses do not change after the epoch of accretion. In order to maintain self-consistency for the latter method, we use full merger trees (from L80G, the simulation described in §3.2.1) to keep track of satellites and to assure that, e.g., mergers between satellites before they reach the central halo preserve stellar mass.

Finally, we note that any specific halo–finding algorithm may introduce artifacts in the halo mass function in terms of when a satellite halo is considered absorbed/destroyed. This can have a small effect on satellite clustering as well as

number density counts. Wetzel & White (2009) suggest an approach that avoids some of the problems associated with resolving satellites after accretion. Namely, they suggest a model where satellites remain in orbit for a duration that is a function of the satellite mass, the host mass, and the Hubble time, after which time they dissolve or merge with the central object. Although we have not modeled this explicitly, our satellite counts are consistent with their recommended cutoff — they suggest considering a satellite halo absorbed when its present mass is less than 0.03 times its infall mass; in our simulation, only 0.1% of all satellites fall below this threshold.

3.4. *Functional Forms for the Stellar Mass – Halo Mass Relation*

In order to determine the probability distribution of our underlying model parameters, we must first define an allowed parameter space for the stellar mass – halo mass relation. Ideally, one would like a simple, accurate, physically intuitive, and orthogonal parameterization; in practice, we seek the best compromise with these four goals in mind. We consider one of the most popular methods for choosing a functional form (indirect parameterization via the stellar mass function) before discussing the method we use in this paper (parameterization via deconvolution of the stellar mass function).

3.4.1. *Parameterizing the Stellar Mass Function*

In abundance matching, knowledge of the halo mass function and the stellar mass function uniquely determines the stellar mass – halo mass relation. Hence, parameterizing the stellar mass function yields an indirect parameterization for the stellar mass – halo mass relation as well. Numerous papers (e.g. Cole et al. 2001; Bell et al. 2003; Panter et al. 2004; Pérez-González et al. 2008) have found that the GSMF is well-approximated by a Schechter function:

$$\phi(M_*, z) = \phi^\star(z) \left(\frac{M_*}{M(z)} \right)^{-\alpha(z)} \exp\left(-\frac{M_*}{M(z)} \right), \qquad (16)$$

where the Schechter parameters $\phi^\star(z)$, $M(z)$, and $\alpha(z)$ evolve as functions of the redshift z. In many previous works on abundance matching (e.g. Conroy et al. 2009), it is the Schechter function for the stellar mass function that sets the form of the SM–HM relation.

More recently, however, several authors have noted that the GSMF cannot be matched by a single Schechter function for $z < 0.2$ to within statistical errors (e.g. Li & White 2009; Baldry et al. 2008), in part because of an upturn in the slope of the GSMF for galaxies below 10^9 $M_\odot$ in stellar mass. It is possible that a conspiracy of systematic errors causes the observed deviations, but there is no fundamental reason to expect the intrinsic GSMF to be fit exactly by a Schechter function (see discussion in Appendix C). In any case, our full parameterization —either the stellar mass function or the error parameterization — *must* be able to capture all the subtleties of the observed stellar mass function. Hence, we are inclined to adopt a more flexible model than the Schechter function of equation 16. Other authors, wrestling with the same problem, have chosen to adopt multiple Schechter functions, including the eleven-parameter triple piecewise Schechter-function fit used by Li & White (2009). While accurate, these models often add complication without increasing intuition.

3.4.2. *Deconvolving the Observed Stellar Mass Function*
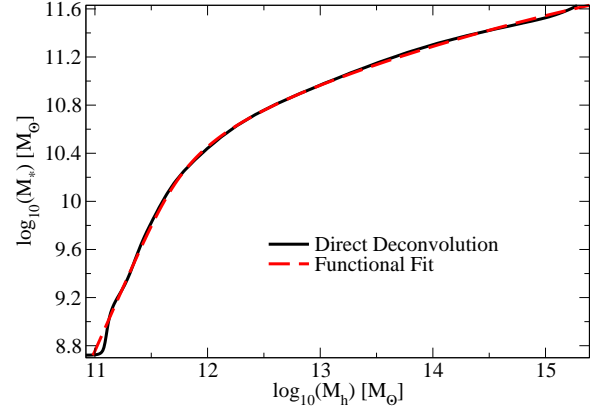

Figure 2. Relation between halo mass and stellar mass in the local Universe, obtained via direct deconvolution of the stellar mass function in Li & White (2009) matched to halos in a WMAP5 cosmology. The deconvolution includes the most likely value of scatter in stellar mass at a given halo mass as well as statistical errors in individual stellar masses. The direct deconvolution (*solid line*) is compared to the best fit to Eq. 21 (*red dashed line*).

Rather than attempting to parameterize the stellar mass function, we could use abundance matching directly to derive the stellar mass – halo mass relation for the maximal-likelihood stellar mass function, and then find a fit which can parameterize the uncertainties in the shape of the relation. This process is complicated by the various errors which we must take into account. Recall from Equations 2 and 13 that

$$\phi_{\rm meas}(M_*) = \phi_{\rm direct}(M_*) \circ P_s(\Delta \log_{10} M_*) \circ P(\Delta \log_{10} M_*), \qquad (17)$$

(where "$\circ$" denotes the convolution operation, P_s is the probability distribution for the scatter in stellar mass at fixed halo mass, and P is the probability distribution for errors in observed stellar mass at fixed true stellar mass). However, if we obtain $\phi_{\rm direct}$ by deconvolution of the observed stellar mass function $\phi_{\rm meas}$, we may use direct abundance matching (Equation 15) to determine the maximum likelihood form of $M_h(M_*)$.

Figure 2 shows the result of calculating $M_h(M_*)$ at $z \sim 0.1$ via deconvolution and direct matching of the stellar mass function as described in the previous section. We choose the maximum-likelihood value for the distribution function P_s (namely, 0.16 dex log-normal scatter), and we use WMAP5 cosmology for the halo mass function ϕ_h in the derivation.

While deconvolution plus direct abundance matching gives an unbiased calculation of the relation, there are several problems which prevent it from being used directly to calculate uncertainties:

1. Deconvolution will tend to amplify statistical variations in the stellar mass function—that is, shallow bumps in the GSMF will be interpreted as convolutions of a sharper feature.

2. Deconvolution will give different results depending on the boundary conditions imposed on the stellar mass function (i.e., how the GSMF is extrapolated beyond the reported data points)—the effects of which may be seen at the edges of the deconvolution in Figure 2.

3. Deconvolution becomes substantially more problem-

atic when the convolution function varies over the redshift range, as it does for our higher-redshift data ($z >$ 0.2).

4. Deconvolution cannot extract the relation at a single redshift—instead, it will only return the relation averaged over the redshift range of galaxies in the reported GSMF.

For these reasons, we choose to find a fitting formula instead. In the discussion that follows, we fit $M_h(M_*)$ (the halo mass for which the average stellar mass is M_*) rather than the more intuitive $M_*(M_h)$ (the average stellar mass at a halo mass M_h) primarily for reasons of computational efficiency. From Equations 12 and 17, the calculation of what observers would see (ϕ_{meas}) for a trial stellar mass – halo mass relation requires many evaluations of $M_h(M_*)$ and no evaluations of $M_*(M_h)$. If we had instead parameterized $M_*(M_h)$, and then inverted as necessary in the calculation of ϕ_{meas}, our calculations would have taken an order of magnitude more computer time.

3.4.3. *Fitting the Deconvolved Relation*

It is well-known from comparing the GSMF (or the luminosity function) to the halo mass function that high-mass ($M_* \gtrsim 10^{10.5}\ M_\odot$) galaxies have a significantly different stellar mass-halo mass scaling than low-mass galaxies, which is usually attributed to different feedback mechanisms dominating in high-mass vs. low-mass galaxies. The transition point between low-mass and high-mass galaxies—seen as a turnover in the plot of $M_h(M_*)$ around $M_* = 10^{10.6}\ M_\odot$ in Figure 2—defines a characteristic stellar mass ($M_{*,0}$) and an associated characteristic halo mass (M_1). Hence, we consider functional forms which respect this general structure of a low stellar mass regime and a high stellar mass regime with a characteristic transition point:

$$\log_{10}(M_h(M_*)) = \quad \log_{10}(M_1) \quad \text{[Characteristic Halo Mass]}$$
$$+ f_{low}(M_*/M_{*,0}) \ \text{[Low-mass functional form]}$$
$$+ f_{high}(M_*/M_{*,0}) \ \text{[High-mass functional form]}$$

where f_{low} and f_{high} are dimensionless functions dominating below and above $M_{*,0}$, respectively.

For low-mass galaxies ($M_* < 10^{10.5}\ M_\odot$), we find the stellar mass – halo mass relation to be consistent with a power–law:

$$\frac{M_h(M_*)}{M_1} \approx \left(\frac{M_*}{M_{*,0}}\right)^\beta,\ \text{or}$$

$$\log(M_h(M_*)) \approx \log(M_1) + \beta \log\left(\frac{M_*}{M_{*,0}}\right). \quad (18)$$

For high-mass galaxies, we find the stellar mass–halo mass relation to be *inconsistent* with a power–law. In particular, the logarithmic slope of $M_h(M_*)$ changes with M_*, with $d\log M_h/d\log M_*$ always increasing as M_* increases. This may seem like a small detail; after all, by eye, it appears that a power law could be a reasonable fit for high-mass galaxies in Figure 2. In addition, because previous authors (e.g., Moster et al. 2009; Yang et al. 2009a) have used power laws, it may not seem necessary to use a different functional form.

In order to explore this issue, we tried a general double power–law functional form for $M_h(M_*)$ which parameterized a superset of the fits used in Moster et al. (2009) and Yang et al. (2009a) (in particular, the same form as in Equation C2 in Appendix C). We found that this approach had two major problems common to any such power–law form:

1. As the logarithmic slope of $M_h(M_*)$ increases with increasing M_*, the best-fit power–law for high-mass galaxies will depend on the upper limit of M_* in the available data for the GSMF. Thus, the best-fit power–law will depend on the number density limit of the observational survey used—rather than on any fundamental physics. Moreover, for studies such as this one which consider redshift evolution, the different number densities probed at different redshifts result in a completely artificial "evolution" of the best-fit power–law.

2. The best–fit power–law will not depend on the highest mass galaxies alone; instead, it will be something of an average over all the high-mass galaxies. Because the logarithmic slope is increasing with M_*, this means that the best-fit power law for $M_h(M_*)$ will increasingly underestimate the true $M_h(M_*)$ at high M_*. Namely, the fit will underestimate the halo mass corresponding to a given stellar mass, and therefore (as lower-mass halos have higher number densities) result in stellar mass functions *systematically* biased above observational values. However, a systematic bias in our functional form will influence the best-fit values of the systematic error parameters. The systematic bias caused by assuming a power–law form turns out to be most degenerate with the scatter in stellar mass at fixed halo mass (ξ). As a result, for the MCMC chains which assumed a double power–law form for $M_h(M_*)$, the posterior distribution of ξ was 0.09 ± 0.02 dex, which just barely lies within 2σ of the constraints from More et al. (2009).

These problems are not as significant if one only considers the stellar mass function at a single redshift, or if one does not allow for the systematic errors which change the overall shape of the stellar mass function (κ, ξ, and $\sigma(z)$). However, we find that the issues listed above exclude the use of a power–law for our purposes. Instead, we find that $M_h(M_*)$ asymptotes to a *sub-exponential* function for high M_*, namely, a function which climbs more rapidly than any power–law function, but less rapidly than any exponential function. We find that high–mass galaxies ($M_* > 10^{10.5}\ M_\odot$) are well fit by the relation

$$M_h(M_*) \stackrel{\sim}{\propto} 10^{\left(\frac{M_*}{M_{*,0}}\right)^\delta},\ \text{or}$$

$$\log_{10}(M_h(M_*)) \to \log_{10}(M_1) + \left(\frac{M_*}{M_{*,0}}\right)^\delta \quad (19)$$

where δ sets how rapidly the function climbs; $\delta \to 0$ would correspond to a power–law, and $\delta = 1$ would correspond to a pure exponential. Typical values of δ at $z = 0$ range from $0.5 - 0.6$. It is not obvious what physical meaning can be directly inferred from the choice of a sub-exponential function—after all, the stellar mass of a galaxy is a complicated integral over the merger and evolution history of the galaxy—but it could suggest that the physics driving the $M_h(M_*)$ relation at high–mass is not scale–free.

Although this form now matches the asymptotic behavior for the highest and lowest stellar mass galaxies, one additional parameter is necessary to match the functional form of the deconvolution. That is to say, galaxies in between the extremes in stellar mass will lie in a transition region, as they may have been substantially affected by multiple feedback mechanisms. The width of this transition region will depend on many things—e.g., how long galaxies take to gain stellar

mass, how much of the stellar mass present came from quiescent star formation as opposed to mergers, and the degree of interaction between multiple feedback mechanisms. Hence, instead of having $M_h(M_*)$ become suddenly sub-exponential for galaxies larger than $M_{*,0}$, we allow for a slow "turn-on" of the more rapid growth. The behavior of $M_h(M_*)$ is best fit by modifying the previous equation to

$$\log_{10}(M_h(M_*)) \rightarrow \log_{10}(M_1) + \frac{\left(\frac{M_*}{M_{*,0}}\right)^\delta}{1 + \left(\frac{M_*}{M_{*,0}}\right)^{-\gamma}} \quad (20)$$

The denominator, $1 + (M_*/M_{*,0})^{-\gamma}$, is large for $M_* < M_{*,0}$, and it falls to unity for $M_* > M_{*,0}$ at a rate controlled by γ. A larger value of γ implies a more rapid transition between the power–law and sub-exponential behavior (typical values for (γ) at $z = 0$ are 1.3-1.7). As the non-constant piece of $M_h(M_*)$ in Equation 20 is $\frac{1}{2}$ for $M_* = M_{*,0}$, we add a final factor of $-\frac{1}{2}$ to compensate so that $M_h(M_{*,0}) = M_1$.

To summarize, our resulting best–fit functional form has five parameters:

$$\log_{10}(M_h(M_*)) =$$

$$\log_{10}(M_1) + \beta \log_{10}\left(\frac{M_*}{M_{*,0}}\right) + \frac{\left(\frac{M_*}{M_{*,0}}\right)^\delta}{1 + \left(\frac{M_*}{M_{*,0}}\right)^{-\gamma}} - \frac{1}{2}. \quad (21)$$

Where M_1 is a characteristic halo mass, $M_{*,0}$ is a characteristic stellar mass, β is the faint-end slope, and δ and γ control the massive-end slope. The best fit using this functional form is shown in Figure 2, and it achieves excellent agreement over the entire range of stellar masses.

Deconvolving the GSMF at higher redshifts does not suggest that anything more than linear evolution in the parameters is necessary, at least out to $z = 1$. While the characteristic mass of the GSMF and the characteristic mass of the halo mass function certainly evolve, the change in the *shapes* of the two functions is relatively slight. As we wish for the functional form to have a natural extension to higher redshifts, we parameterize the evolution in terms of the scale factor (a):

$$\begin{aligned}
\log_{10}(M_1(a)) &= M_{1,0} + M_{1,a}(a-1), \\
\log_{10}(M_{*,0}(a)) &= M_{*,0,0} + M_{*,0,a}(a-1), \\
\beta(a) &= \beta_0 + \beta_a(a-1), \quad (22) \\
\delta(a) &= \delta_0 + \delta_a(a-1), \\
\gamma(a) &= \gamma_0 + \gamma_a(a-1),
\end{aligned}$$

where $a = 1$ is the scale factor today.

3.5. *Calculating Model Likelihoods*

We make use of a Markov Chain Monte Carlo (MCMC) method to generate a probability distribution in our complete parameter space of stellar mass function parameters ($M_{1,0}, M_{1,a}, M_{*,0,0}, M_{*,0,a}, \beta_0, \beta_a, \delta_0, \delta_a, \gamma_0, \gamma_a$), systematic modeling errors (κ, μ, σ_z), and the scatter in stellar mass at fixed halo mass (ξ). A brief summary of each of these parameters appears in Table 1 along with a reference to the section in which it was first described. Using this full model, we may calculate the stellar mass functions expected to be seen by observers ($\phi_{\rm expect}$) for a large number of points in parameter space, and compare them to observed GSMFs (Li & White

2009; Pérez-González et al. 2008). Note that, as the observational data always covers a range of redshifts, we must mimic this in our calculation of $\phi_{\rm expect}$:

$$\phi_{\rm expect} = \frac{\int_{z_1}^{z_2} \phi_{\rm fit}(z) dV_C(z)}{\int_{z_1}^{z_2} dV_C(z)}, \quad (23)$$

where $dV_C(z)$ is the comoving volume element per unit solid angle as a function of redshift. Then, we can write the likelihood as $\mathcal{L} = \exp\left(-\chi^2/2\right)$, where

$$\chi^2 = \int \left[\frac{\log_{10}[\phi_{\rm expect}(M_*)/\phi_{\rm meas}(M_*)]}{\sigma_{\rm obs}(M_*)}\right]^2 d\log_{10}(M_*), \quad (24)$$

and where $\sigma_{\rm obs}(M_*)$ is the reported statistical error in $\phi_{\rm meas}$ as a function of stellar mass.

Note that, as defined above, the equation for χ^2 contains the assumption that there is only one independent observation point for the GSMF per decade in stellar mass (from the weight of $d\log_{10}(M)$). We may tune this assumption introducing another parameter n—the number of non-correlated observations per decade in stellar mass—which would change the likelihood function to $\mathcal{L} = \exp\left(-n\chi^2/2\right)$. Here, we assume that each of the data points reported by Li & White (2009) and Pérez-González et al. (2008) are independent—such that $n = 10$ for the former paper and $n = 5$ for the latter paper.

The MCMC chains each contain $2^{22} \approx 4 \times 10^6$ points. We verify convergence according to the algorithm in Dunkley et al. (2005); in all cases, the ratio of the sample mean variance to the distribution variance (the "convergence ratio") is below 0.005.

3.6. *Methodology Summary*

Our procedure to calculate the stellar mass – halo mass relation, taking into account all mentioned uncertainties, may be summarized in seven steps:

1. We select a trial point in the parameter space of SM–HM relations as well as a trial point in our parameter space of systematics (μ, κ, σ_z, ξ). A complete list of parameters and descriptions is given in Table 1.

2. The trial SM–HM relation gives a one-to-one mapping between halo masses and stellar masses, giving a direct conversion from the halo mass function to a trial galaxy stellar mass function (corresponding to $\phi_{\rm direct}$ in §3.3.1).

3. This trial GSMF is convolved with the probability distributions for scatter in stellar mass at fixed halo mass (controlled by ξ, see §3.3.1) and for scatter in observer-determined stellar mass at fixed true stellar mass (partially controlled by σ_z, see §3.1.2).

4. The resulting GSMF is shifted by a uniform offset in stellar masses (controlled by μ) to account for uniform systematic differences between our adopted stellar masses and the true underlying masses. Also, its shape is stretched or compressed to account for stellar mass–dependent offsets between our masses and the true underlying masses (controlled by κ, see §3.1.1).

5. We repeat steps 2-4 for all redshifts in the range covered by the observed data set. We may then calculate

Table 1
Summary of Model Parameters

Symbol	Description	Prior[a]	Section
$M_h(M_*)$	The halo mass for which the average stellar mass is M_*	N/A	3.4.3
M_1	Characteristic Halo Mass	Flat (Log)	3.4.3
$M_{*,0}$	Characteristic Stellar Mass	Flat (Log)	3.4.3
β	Faint-end power law ($M_h \sim M_*^\beta$)	Flat (Linear)	3.4.3
δ	Massive-end sub-exponential ($\log_{10}(M_h) \sim M_*^\delta$)	Flat (Linear)	3.4.3
γ	Transition width between faint- and massive-end relations	Flat (Linear)	3.4.3
$(x)_0$	Value of the variable (x) at the present epoch, where (x) is one of $(M_1, M_{*,0}, \beta, \delta, \gamma)$	(see above)	3.4.3
$(x)_a$	Evolution of the variable (x) with scale factor	(same as for $(x)_0$)	3.4.3
μ	Systematic offset in M_* calculations	$G(0, 0.25)$ (Log)	3.1.1
κ	Systematic mass-dependent offset in M_* calculations	$G(0, 0.10)$ (Linear)	3.1.1
σ_z	Redshift scaling of statistical errors in M_* calculations	$G(0.05, 0.015)$ (Log)	3.1.2
ξ	Scatter in M_* at fixed M_h	$G(0.16, 0.04)$ (Log)	3.3.1

[a] See Equations 1, 5, 21-23. $G(x,s)$ denotes a Gaussian prior centered at x with standard deviation s, in either linear or logarithmic units. 'Flat' denotes a uniform prior in either linear or logarithmic units.

the expected GSMF in each redshift bin for which observers have reported data. The likelihood of the expected GSMFs given the measured GSMFs is then used to determine the next step in the MCMC chain.

6. To account for sample variance in the observed stellar mass functions above $z \sim 0.2$, we recalculate each SM–HM relation in the chain for an alternate halo mass function taken from a randomly sampled mock survey (see §3.2.4) and re-fit our functional form to the redshift evolution of the relation. Similarly, for the results which include cosmology uncertainty, we recalculate each SM–HM relation for an alternate halo mass function randomly selected from the MCMC chain used to determine the WMAP5 cosmology uncertainties.

7. We repeat steps 1-6 to build a joint probability distribution for the SM–HM relation and the systematics parameter space. The steps are repeated until the joint probability distribution has converged to the underlying posterior distribution.

4. RESULTS FOR $0 < z < 1$

We now present the results of this approach to determine the SM–HM relation and related quantities. In §4.1, we compare GSMFs generated from our best fits to observed data and comment on the effects of systematic observational biases. We present our best-fitting results for the SM–HM relation with full error bars in §4.2. We evaluate the relative importance of each of the contributing types of error in §4.3 and summarize the most relevant contributions in §4.3.7. Finally, our derived SM–HM relation is compared to other published results in §4.4.

4.1. *Galaxy Stellar Mass Functions*

To demonstrate that our functional form for $M_h(M_*)$ is capable of reproducing observed galaxy stellar mass functions, we show a comparison between our best–fit models and the observed data in Figs. 3 and 4 at several redshifts. For our best-fit models, both $\phi_{\rm true}$ (the true or "intrinsic" stellar mass function) and $\phi_{\rm meas}$ (the GSMF that observers would measure) are shown. Recall that $\phi_{\rm meas}$ incorporates the effects of the systematic observational biases; namely, the overall shift in stellar mass calculations, μ, the linearly mass-dependent shift, κ, and the statistical errors in stellar mass calculations for individual galaxies, $\sigma(z)$. The fact that the best-values of the

systematic parameters (μ, κ, ξ, σ_z) are very close to the centers of their prior distributions provides confirmation that the functional form for the SM–HM relation outlined in §3.4.3 does not bias our best-fit results.

As our best-fit values for μ and κ are close to zero (see Table 2), the difference between $\phi_{\rm true}$ and $\phi_{\rm meas}$ is almost exclusively due to the scatter $\sigma(z)$ in calculated stellar masses. The difference between $\phi_{\rm true}$ and $\phi_{\rm meas}$ only becomes evident for galaxies above $10^{11}\ M_\odot$, where the falling slope of the GSMF becomes severe enough for the scatter $\sigma(z)$ to significantly raise number counts in the observed GSMF. At $z \sim 0$, the systematic effect of $\sigma(z)$ puts the intrinsic GSMF well below the small statistical error bars.

At higher redshifts, although the effect of $\sigma(z)$ is larger, current surveys at $z > 0.2$ do not yet cover sufficient volume to constrain the shape of the GSMF well at the massive end. Nonetheless, for future wide-field surveys at $z > 0.2$, correction to the GSMF for scatter in calculated stellar masses will be an important consideration.

4.2. *The Best-Fit Stellar Mass – Halo Mass Relations*

We plot the average stellar mass as a function of halo mass for $z = 0 - 1$ in Figure 5 to show the evolution of the stellar mass – halo mass relation. Note that as the stellar mass at a given halo mass has a log-normal scatter (see §2.3), we use geometric averages for stellar masses rather than linear ones. To highlight the effects of halo mass on star formation efficiency, we also present the SM–HM relation in terms of the average stellar mass fraction (stellar mass / halo mass) for $z = 0 - 1$ as a function of halo mass in the same figure. We focus on this quantity for the remainder of the paper. The best-fit parameters for the function $M_h(M_*)$ are given in Table 2, and the numerical values for the stellar mass fractions are listed in Appendix D.

The stellar mass fractions for central galaxies consistently show a maximum for halo masses near $10^{12}\ M_\odot$. While the location of this maximum evolves with time, it clearly illustrates that star-formation efficiency must fall off for both higher and lower-mass halos. The slopes of the SM–HM relation above and below this characteristic halo mass are indicative of at least two processes limiting star-formation efficiency, although mergers complicate direct analysis for high-mass halos. At the low-mass end, the SM–HM relation scales as $M_* \sim M_h^{2.3}$ at $z = 0$ and as $M_* \sim M_h^{2.9}$ at $z = 1$. However, given the lack of information about low stellar-mass galaxies at $z > 0.5$, the statistical significance of this evolution is weak;
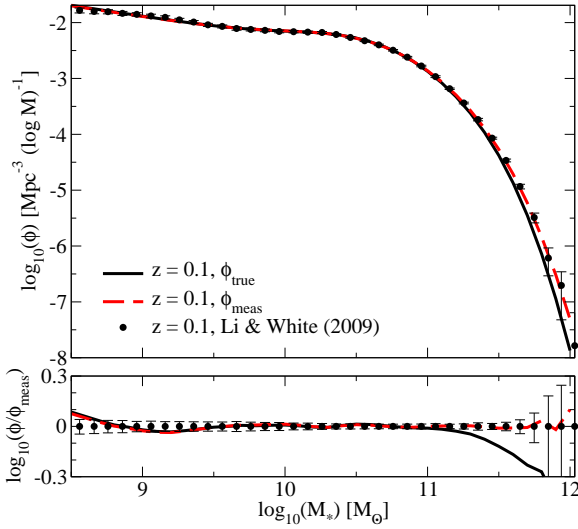
Figure 3. Comparison of the best fit $\phi_{\rm true}$ (the true or "intrinsic" GSMF) in our model to the resulting $\phi_{\rm meas}$ (what an observer would report for the GSMF, which includes the effects of the systematic biases μ, κ, and σ) at $z = 0$. Since the best–fit values of μ and κ are very close to zero, the difference between $\phi_{\rm meas}$ and $\phi_{\rm true}$ almost exclusively comes from the uncertainty in measuring stellar masses (σ).

Table 2
Best fits for the redshift evolution of $M_h(M_*)$

Parameter	Free (μ, κ) $0 < z < 1$	$\mu = \kappa = 0$ $0 < z < 1$	Free (μ, κ) $0.8 < z < 4$
$M_{*,0,0}$	$10.72^{+0.22}_{-0.29}$	$10.72^{+0.02}_{-0.12}$	$11.09^{+0.54}_{-0.31}$
$M_{*,0,a}$	$0.55^{+0.18}_{-0.79}$	$0.59^{+0.15}_{-0.85}$	$0.56^{+0.89}_{-0.44}$
$M_{*,0,a^2}$	N/A	N/A	$6.99^{+2.69}_{-3.51}$
$M_{1,0}$	$12.35^{+0.07}_{-0.16}$	$12.35^{+0.02}_{-0.15}$	$12.27^{+0.59}_{-0.27}$
$M_{1,a}$	$0.28^{+0.19}_{-0.97}$	$0.30^{+0.14}_{-1.02}$	$-0.84^{+0.87}_{-0.58}$
β_0	$0.44^{+0.04}_{-0.06}$	$0.43^{+0.01}_{-0.05}$	$0.65^{+0.26}_{-0.20}$
β_a	$0.18^{+0.08}_{-0.34}$	$0.18^{+0.06}_{-0.34}$	$0.31^{+0.38}_{-0.47}$
δ_0	$0.57^{+0.15}_{-0.06}$	$0.56^{+0.06}_{-0.05}$	$0.56^{+1.33}_{-0.29}$
δ_a	$0.17^{+0.42}_{-0.41}$	$0.18^{+0.41}_{-0.42}$	$-0.12^{+0.76}_{-0.50}$
γ_0	$1.56^{+0.12}_{-0.38}$	$1.54^{+0.03}_{-0.40}$	$1.12^{+7.47}_{-0.36}$
γ_a	$2.51^{+0.15}_{-1.83}$	$2.52^{+0.03}_{-1.89}$	$-0.53^{+7.87}_{-2.50}$
μ	$0.00^{+0.24}_{-0.25}$	N/A	$0.00^{+0.25}_{-0.25}$
κ	$0.02^{+0.11}_{-0.07}$	N/A	$0.00^{+0.14}_{-0.04}$
ξ	$0.15^{+0.04}_{-0.02}$	$0.15^{+0.04}_{-0.01}$	$0.16^{+0.07}_{-0.01}$
σ_z	$0.05^{+0.02}_{-0.01}$	$0.05^{+0.02}_{-0.01}$	$0.05^{+0.02}_{-0.01}$

Note. — See Table 1 and Equations 1, 5, 21-23, 25.

no evolution in the low-mass slope of the relation is consistent within our one-sigma errors. Several studies (most recently, Baldry et al. 2008; Drory et al. 2009) have reported that the GSMF has an upturn in slope for very low stellar masses, particularly below $10^{8.5}M_\odot$; this would imply that our best fits may overestimate the scaling relation for galaxies below $10^{8.5}M_\odot$. At the high mass end, our best fitting function results in a progressively shallower relation for the growth of stellar mass with halo mass, so that no single power law can describe the scaling. However, for halos close to $10^{14}M_\odot$, the best-fit relation scales locally as $M_* \sim M_h^{0.28}$ at $z = 0$ and
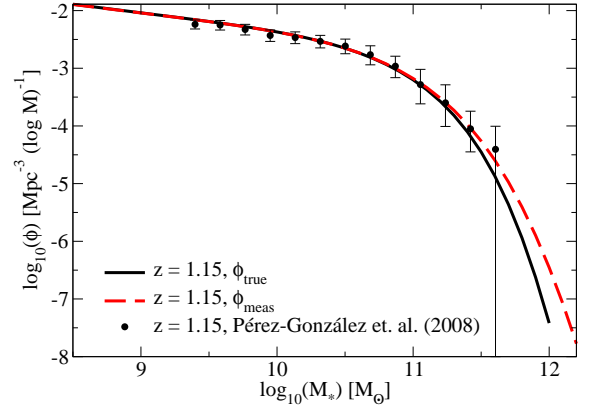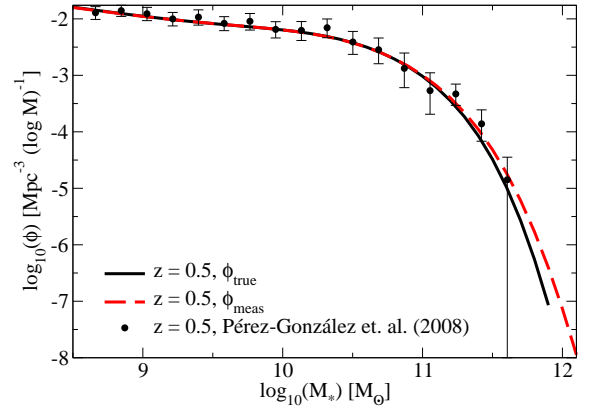

Figure 4. Comparison of the best fit $\phi_{\rm true}$ (the true or "intrinsic" GSMF) to the resulting $\phi_{\rm meas}$ (as in Figure 3), for $z = 0.5$ and $z = 1.15$. Statistical errors in individual stellar masses have a larger effect at higher redshift, resulting in a steeper intrinsic bright end than measured.

$M_* \sim M_h^{0.34}$ at $z = 1$, in accord with previous studies (see §4.4). The results for high mass halos are also consistent with no evolution in the slope of the SM–HM relation.

Figure 6 shows the stellar mass fraction for $0 < z < 1$ excluding the effects of systematic shifts in stellar mass calculations (i.e., assuming $\mu = \kappa = 0$). Under the assumption that systematic errors in stellar mass calculations result in similar biases in stellar masses at $z = 0$ as they do at higher redshifts, this allows us to consider the evolution in normalization of the SM–HM relation. Low-mass halos (below 10^{12} $M_\odot$) display clearly higher stellar mass fractions at late redshifts than they do at early redshifts. By contrast, the evolution in stellar mass fractions for high mass halos (above $10^{13.5}$ $M_\odot$) is not statistically significant, and it is constrained to be substantially less than for low-mass halos. In the time since $z = 1$, this means that the star formation rates for high-mass halos typically fall relative to their dark matter accretion rates, whereas the opposite is true for low-mass halos (Conroy & Wechsler 2009). The best-fitting parameters for the SM–HM relation assuming $\mu = \kappa = 0$ appear in Table 2, and the data points in Figure 6 appear in Appendix D.
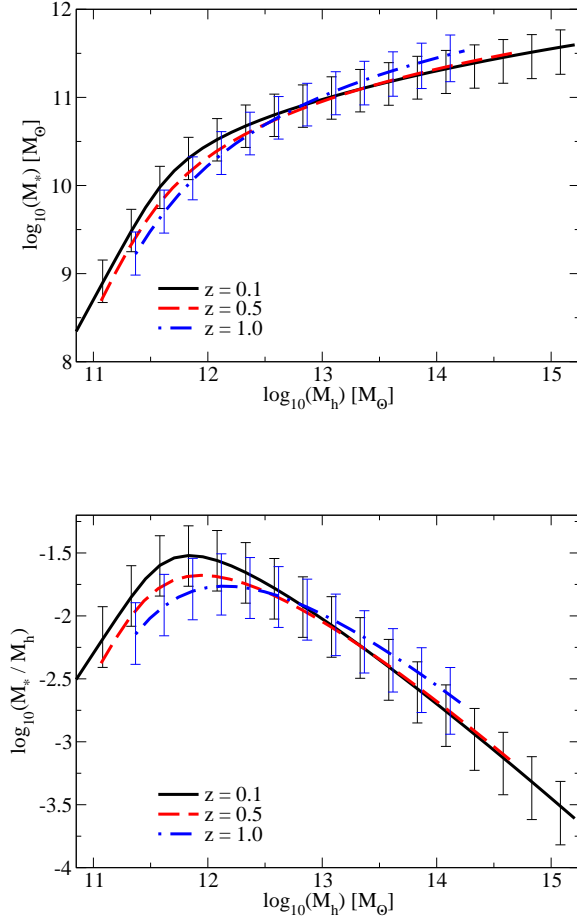
4.3. *Impact of Uncertainties*

Figure 6. Evolution of the derived stellar mass fractions (M_*/M_h) in the absence of systematic errors. This result is analogous to Figure 5, bottom panel, calculated under the assumption that the true values of the systematics μ and κ in the stellar mass function are zero at all redshifts.

ter to have significant impact (see also Tasitsiomi et al. 2004). Because $\xi > 0$ results in high stellar–mass galaxies being assigned to lower-mass halos than they would be otherwise (due to the higher number density of lower-mass halos), the effect is that higher-mass halos contain fewer stars on average than they would for $\xi = 0$. The effect of setting $\xi = 0$ exceeds systematic error bars only for the very highest mass halos, above $10^{14.5}$ $M_\odot$.

We note that our posterior distribution constrains ξ to be less than 0.22 dex at the 98% confidence level. Higher values for ξ would result in GSMFs inconsistent with the steep falloff of the Li & White (2009) GSMF (see also discussion in Guo et al. 2009).

4.3.3. *Statistical Errors in Stellar Mass Calculations*

The significance of including or excluding random statistical errors in stellar mass calculations, $\sigma(z)$, is also shown Figure 7. The effect of this type of scatter on the SM–HM relation is mathematically identical to the effect of scatter in stellar mass at fixed halo mass. As $\sigma(z = 0)$ (~ 0.07 dex) is much smaller than the expected value of ξ (~ 0.16 dex), the convolution of the two effects is only marginally different from including ξ alone at $z = 0$; this results in only a minor effect on the SM–HM relation. The effect becomes more pronounced at $z = 1$ for the reason that $\sigma(z = 1)$ (~ 0.12 dex) becomes more comparable to ξ—and so including the effects of statistical errors in stellar mass becomes as important as modeling scatter in stellar mass at fixed halo mass.

4.3.4. *Cosmology Uncertainties*

In Figure 8, we show a comparison of best fits for the stellar mass fraction using abundance matching with three different halo mass functions: analytic prescriptions for WMAP5 and WMAP1 (see §3.2.2) as well as the mass function taken directly from the L80G simulation (see §3.2.1). The difference between the L80G simulation and the analytic WMAP1 mass function is slight, as the L80G simulation uses WMAP1 initial conditions ($h = 0.7$, $\Omega_m = 0.3$, $\Omega_\Lambda = 0.7$, $\sigma_8 = 0.9$, $n_s = 1$); the difference is consistent with sample variance for the relatively small (80 h^{-1} Mpc) size of the simulation. The difference between SM–HM relations using WMAP1 and WMAP5 cos-

Figure 5. *Top panel*: Stellar mass – halo mass relation as a function of redshift for our preferred model. *Bottom panel*: Evolution of the derived stellar mass fractions (M_*/M_h). In each case, the lines show the mean values for central galaxies. These relations also characterize the satellite galaxy population if the horizontal axis is interpreted as the halo mass at the time of accretion. Errors bars include both systematic and statistical uncertainties, calculated for a fixed cosmological model (with WMAP5 parameters).

4.3.1. *Systematic Shifts in Stellar Mass Calculations*

By far the largest contributor to the error budget of the SM–HM relation is the systematic error parameter μ. As the effect of μ is to multiply all stellar masses by a constant factor, and as the width of the error bars in Figure 5 corresponds almost exactly to the prior on μ, we may conclude that reducing the error on the systematic shifts in stellar mass calculations would represent the single largest improvement in our understanding of the shape of the SM–HM relation. Figure 6 shows the substantially smaller error bars that result if systematic errors (μ and κ) in the stellar mass calculations are neglected.

4.3.2. *Scatter in Stellar Mass at Fixed Halo Mass*

The effect of ignoring scatter in stellar mass at fixed halo mass (i.e., setting $\xi = 0$) is shown at two redshifts in Figure 7. We find that the change is insignificant below halo masses of 10^{12} $M_\odot$, and is within statistical error bars below 10^{13} $M_\odot$ for $z = 1$. This is a result of the fact that the slope of the stellar mass function below $10^{10.5}$ $M_\odot$ in stellar mass (corresponding to 10^{12} $M_\odot$ in halo mass) is not steep enough for scat-
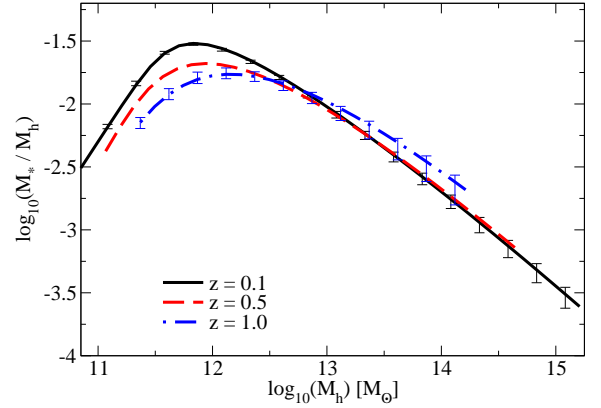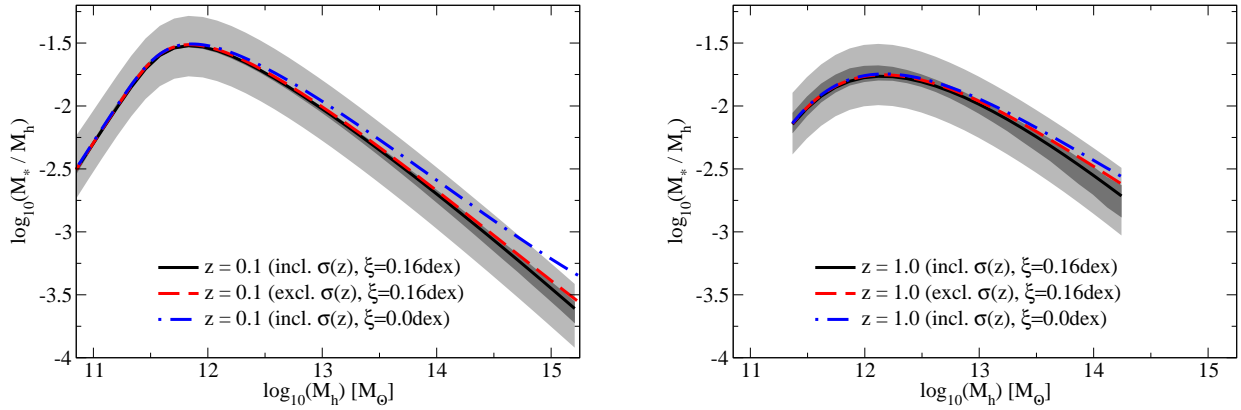
Figure 7. Comparison between SM–HM relations derived in the preferred model (including the effects of the statistical errors $\sigma(z)$ and taking the scatter in stellar mass at a given halo mass to be $\xi = 0.16$dex) to those excluding the effects of $\sigma(z)$ or taking $\xi = 0$, at $z = 0$ (*left panel*) and $z = 1$ (*right panel*). Light shaded regions denote 1-σ errors including both systematic and statistical errors; dark shaded regions denote the 1-σ errors if the systematic offsets in stellar mass calculations (μ and κ) are fixed to 0.

mologies is within the systematic errors at all masses. When systematic errors are neglected, the two cosmologies yield SM–HM relations that are noticeably different only at low halo masses ($M < 10^{12}M_\odot$).

Figure 9 show the results of including uncertainties in the WMAP5 cosmological parameters. As described in §3.1, this is done using halo mass functions calculated with parameters resampled from the cosmological parameter chains provided by the WMAP team. Only at $z \sim 0$ are the changes in error bars significant enough to justify mention. Here, the uncertainty in cosmology begins to exceed other sources of statistical error for halos below $10^{12}M_\odot$ due to the small errors on the GSMF at the stellar masses associated with such halos (Li & White 2009). However, the cosmology uncertainties are still well within the systematic error bars.

4.3.5. *Sample Variance*

Because of the large volume of the SDSS, sample variance contributes insignificantly to the error budget for the SM–HM relation below $z = 0.2$. Above that redshift, the comparatively limited survey volume of Pérez-González et al. (2008) results in sample variance becoming an important contributor to the statistical error for halos below $10^{12}M_\odot$ (Poisson noise dominates for larger halos). If the effects of sample variance were ignored, the statistical error spreads for our derived SM–HM relations at $z = 1$ would shrink from 0.12 dex to 0.09 dex for $10^{11}M_\odot$ halos, and from 0.05 dex to 0.04 dex for $10^{12.25}M_\odot$ halos. As with other types of errors, these considerations are well below the limits of the systematic error bars.

We caution that our error bars including sample variance at $z > 0$ have a very specific meaning. Namely, they include the standard deviation in our *fitting form* which might be expected if the survey in Pérez-González et al. (2008) had been conducted on alternate patches of the sky. Sample variance at redshifts $z > 0$ impacts only the linear evolution of the SM–HM relations we derive, as the large volume probed by the SDSS constrains the SM–HM relation very well at $z \sim 0$. Because our fit is matched to the ensemble of reported data between $0 < z < 1$, it is less vulnerable to the effects of sample variance in individual redshift bins. Instead, it is affected most by overall shifts in the number densities reported for the en-

tire high-redshift survey. While this means that our fit gives a more robust SM–HM relation at all redshifts, some caution must be used when comparing our relation to results derived from the GSMF in a single redshift bin (e.g., $0.2 < z < 0.4$). These will have much larger uncertainties due to sample variance than SM–HM relations derived (like ours) from GSMFs along a light cone probing a large redshift range.

To demonstrate the credibility of our approach for calculating the appropriate error bars including sample variance, we repeated our analysis of the SM–HM relation using GSMFs from Drory et al. (2009) (which appeared as we were completing this work) instead of Pérez-González et al. (2008) for $0.2 < z < 1$ and retaining the GSMF from Li & White (2009) for $z < 0.2$. Although the COSMOS survey in Drory et al. (2009) covers a much larger area ($\sim$9x the area in Pérez-González et al. 2008), the fact that it is a single field means that the expected sample variance is only slightly smaller than for the combined fields in Pérez-González et al. (2008). As might be expected, the SM–HM relation at $z = 0.1$ using the Drory et al. (2009) GSMF is identical to the result in Figure 6 because of the strong constraining power of the SDSS data sample. At $z = 1$, the SM–HM relation generated by using the Drory et al. (2009) GSMF is within our quoted statistical and sample variance errors, as shown in Figure 12. This may not be surprising unless one considers that clustering results suggest an overdensity at the 2-3σ level in the COSMOS redshift bin $z = 1$ (Meneux et al. 2009). However, because our method fits the Drory et al. (2009) GSMFs across the entire redshift range, the excess at $z = 1$ is partially offset by an underdensity at $z = 0.5$. This demonstrates the robustness of our fitting method to the effects of sample variance except on the scale of the entire survey.

4.3.6. *Satellite Treatment*

Finally, we consider the changes in both the stellar mass fraction and total stellar mass fraction (total stellar mass in central galaxy and all satellites / total halo mass) induced by different satellite evolution models (see §3.3.2 for details on the two models). As shown in Figure 10, fixing satellite stellar mass at the redshift of accretion (lines labeled as "SMF$_{acc}$") has virtually no effect on either fraction as compared to allow-
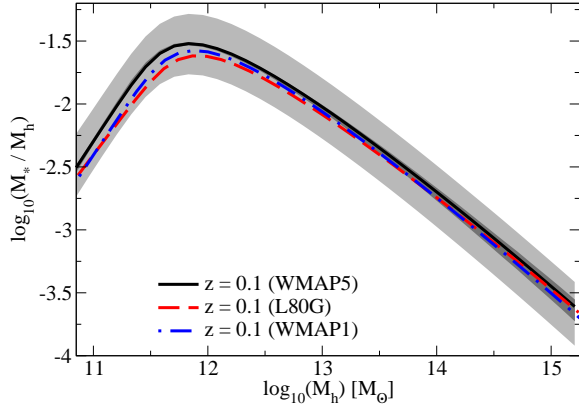
Figure 8. Comparison between stellar mass fractions in different cosmologies. Light shaded regions denote systematic error spreads while dark shaded regions denote error spreads assuming $\mu = \kappa = 0$, both about the WMAP5 model. The dot-dashed blue line shows the fiducial relation for a WMAP1 cosmological model (using our analytic model) The dashed red line shows the relation for a simulation of the WMAP1 cosmology. Differences between this and the analytic model are within the expected sample variance errors.
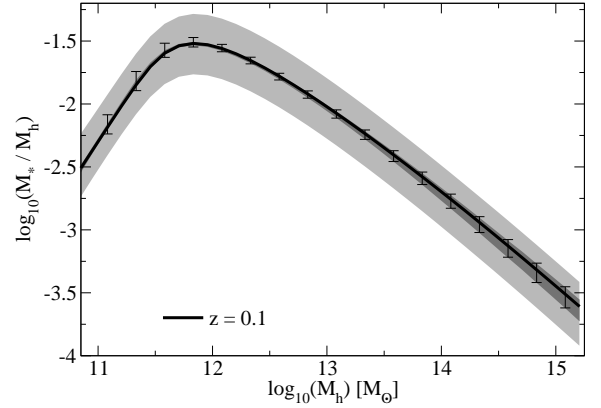

Figure 9. Effect of cosmological uncertainties on the stellar mass fraction at $z = 0.1$. The error bars show the spread in stellar mass fractions including both statistical errors and cosmology uncertainties (from WMAP5 constraints, Komatsu et al. 2009). For comparison, the light shaded region includes statistical and systematic errors, while the dark shaded region includes only statistical errors.

ing satellite stellar mass to evolve the same way as centrals with the same mass (labeled as SMF$_{now}$). Because comparison of different satellite evolution models requires tracking satellites through merger trees, Figure 10 shows results only for satellites in the L80G simulation.

The treatment of satellites may have a somewhat larger impact on the total stellar mass fraction, including the stellar mass of both central and satellite galaxies within a halo. This is shown for both models in Figure 10. Because of the steep fall-off in stellar mass for low mass galaxies, the total stellar mass fraction has only minimal contribution from satellites for low mass halos, and deviates significantly from the stellar mass fraction for centrals only at halo masses $M_h > 10^{12.5} M_\odot$. At cluster-scale masses ($M_h \sim 10^{14} M_\odot$), accreted satellites have on average a higher ratio of stars to dark matter than the central galaxy, and the total stellar mass fraction can be many times the central stellar mass fraction. However, the impact of the two models for satellite treatment on this ratio is small. Profiles of satellite galaxies in clusters should be able to better distinguish between such models.

4.3.7. *Summary of Most Important Uncertainties*

Systematic stellar mass offsets resulting from modeling choices result in the single largest source of uncertainties (~ 0.25 dex at all redshifts). The contribution from all other sources of error is much smaller, ranging from 0.02-0.12 dex at $z = 0$ and from 0.07-0.16 dex at $z = 1$. On the other hand, this statement is only true when all contributing sources of scatter in stellar masses are considered. Models that do not account for scatter in stellar mass at fixed halo mass will overpredict stellar masses in $10^{14.25}$ $M_\odot$ halos by 0.13-0.19 dex, depending on the redshift. Models that do not account for scatter in calculated stellar mass at fixed true stellar mass will overpredict stellar masses in $10^{14.25}$ $M_\odot$ halos by 0.12 dex at $z = 1$. Hence, it is important to take both these effects into account when considering the SM–HM connection either at high masses or at high redshifts.
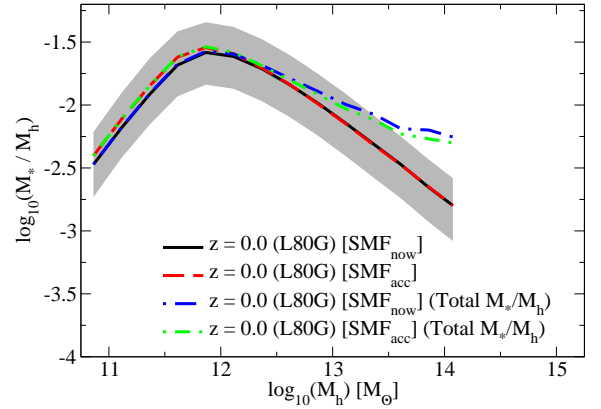

Figure 10. Comparison between stellar mass fractions and total stellar mass fractions (labeled as "Total M_*/M_h") derived by assuming different matching epochs for satellite galaxies. The L80G simulation was used here in order to follow the accretion histories of the subhalos. The relations terminate at high masses where the halo statistics become unreliable due to finite–volume effects.

4.4. *Comparison with other work*

A comparison of our results with several results in the literature at $z \sim 0.1$ is shown in Figure 11. Such comparison is not always straightforward, as other papers have often made different assumptions for the cosmological model, the definition of halo mass, or the measurement of stellar mass. In addition, some papers report the average stellar mass at a given halo mass (as we do), and others report the average halo mass at a given stellar mass. Given the scatter in stellar mass at fixed halo mass, the averaging method can affect the resulting stellar mass fractions, particularly for group- and cluster-scale halo masses. To facilitate comparison with both approaches, we plot our main results (labeled as "$\langle M_*/M_h|M_h\rangle$") along with results for which the stellar mass fractions have been averaged at a given stellar mass (labeled as "$\langle M_*/M_h|M_*\rangle$").
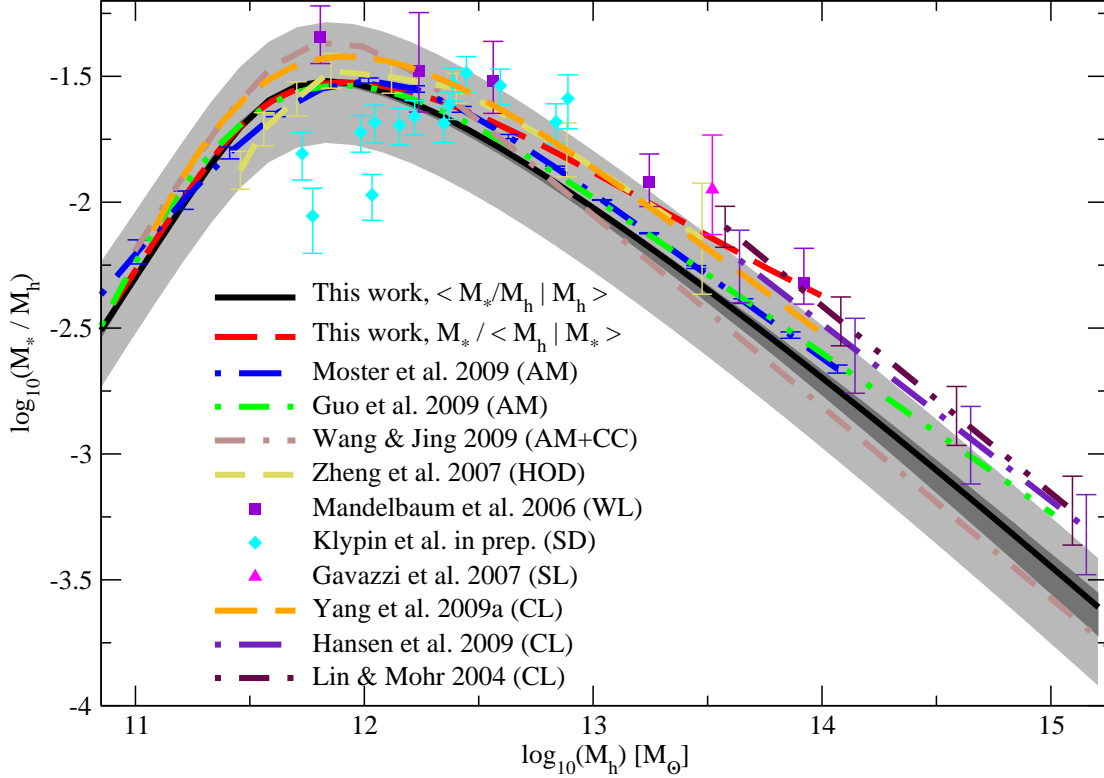
Figure 11. Comparison of our best-fit model at $z = 0.1$ to previously published results. Results shown include other results from abundance matching (Moster et al. 2009 and Guo et al. 2009); abundance matching plus clustering constraints (Wang & Jing 2009); HOD modeling (Zheng et al. 2007); direct measurements from weak lensing (Mandelbaum et al. 2006), statellite dynamics (Klypin et al. 2009) and strong lensing (Gavazzi et al. 2007); and clusters selected from SDSS spectroscopic data (Yang et al. 2009a), SDSS photometric data (the maxBCG sample Hansen et al. 2009), and X-ray selected clusters (Lin & Mohr 2004). Dark grey shading indicates statistical and sample variance errors; light grey shading includes systematic errors. The red line shows our results averaged over stellar mass instead of halo mass; scatter affects these relations differently at high masses. The results of Mandelbaum et al. (2006) and Klypin et al. (2009) are determined by stacking galaxies in bins of stellar mass, and so are more appropriately compared to this red line.

In the comparisons below, we have not adjusted the assumptions used to derive stellar masses, because such adjustments can be complex and difficult to apply using simple conversions. Additionally, we have only corrected for differences in the underlying cosmology for those papers using a variant of abundance matching method (Moster et al. 2009; Guo et al. 2009; Wang & Jing 2009; Conroy et al. 2009) using the process described in Appendix A, as alternate methods require corrections which are much more complicated. We have, however, adjusted the IMF of all quoted stellar masses to that of Chabrier (2003), and we have converted all quoted halo masses to virial masses as defined in §3.2.2.

The closest comparison with our work, using a very similar method, is the result from Moster et al. (2009). This result is in excellent agreement with ours at the high mass end, and is within our systematic errors for all masses considered. However, their less flexible choice of functional form, and their use of a different stellar mass function (estimated from spectroscopy using the results of Panter et al. 2007) results in a different value for the halo mass M_{peak} with peak stellar mass fraction and a shallower scaling of stellar mass with halo mass

at the low mass end. Their error estimates only account for statistical variations in galaxy number counts, and they do not include sample variance or variations in modeling assumptions. Guo et al. (2009) use a similar approach to Moster et al. (2009), using stellar masses from Li & White (2009), but they do not account for scatter in stellar mass at fixed halo mass. Consequently, their results match ours for $10^{12} M_\odot$ and less massive halos, but overpredict the stellar mass for larger halos.

Wang & Jing (2009) use a parameterization for the SM–HM relation for both satellites and centrals, and they attempt to simultaneously fit both the stellar mass function and clustering constraints, including the effects of scatter in stellar mass at fixed halo mass. At $z \sim 0.1$, their data source matches ours (Li & White 2009), but their approach finds a best-fit scatter in stellar mass at fixed halo mass of $\xi = 0.2$ dex, essentially the highest value allowed by the stellar mass function (Guo et al. 2009). As this is higher than our best-fit value for ξ, their SM–HM relation falls below ours for high-mass galaxies. Possibly because of the limited flexibility of their fitting form (they use only a four-parameter double power-law),

their SM–HM relation is in excess of ours for halo masses near $10^{12} M_\odot$.

Zheng et al. (2007) used the galaxy clustering for luminosity-selected samples in the SDSS to constrain the halo occupation distribution. This gives a direct constraint on the r–band luminosity of central galaxies as a function of halo mass. Stellar masses for this sample were determined using the $g - r$ color and the r-band luminosity as given by the Bell et al. (2003) relation, and a WMAP1 cosmology was assumed. This method allows for scatter in the luminosity at fixed halo mass to be constrained as a parameter in the model; results for this scatter are consistent with More et al. (2009), although they are less well constrained. According to Li & White (2009), stellar masses for the Bell et al. (2003) relation are systematically larger than those calculated using Blanton & Roweis (2007) by 0.1–0.3 dex. However, as Ω_m in WMAP1 is larger than in WMAP5, halo masses in WMAP1 will be higher at a given number density than in WMAP5, somewhat compensating for the higher stellar masses.

We next compare to constraints from direct measurements of halo masses from dynamics or gravitational lensing. Mandelbaum et al. (2006) have used weak lensing to measure the galaxy–mass correlation function for SDSS galaxies and derive a mean halo mass as a function of stellar mass. Mandelbaum et al. (2006) assume a WMAP1 cosmology and uses spectroscopic stellar masses, calculated per Kauffmann et al. (2003). Klypin et al (in preparation) have derived the mean halo mass as a function of stellar mass using satellite dynamics of SDSS galaxies (see also Prada et al. 2003; van den Bosch et al. 2004; Conroy et al. 2007). Their results are generally within our systematic errors but lower than others at the lowest masses and with a somewhat different shape. This may be due to selection effects, as their work uses only isolated galaxies, which may have somewhat lower average stellar masses. Gavazzi et al. (2007) use a set of strong lenses from the SLACS survey along with a model for simultaneously fitting the stellar and dark matter components of the stacked lens profiles. This result, at one mass scale, is a bit higher than our error range but within 1.5 σ. The selection effects relevant to strong lenses are beyond the scope of this paper; however, within the effective radius, the stellar mass can easily contribute more to the lensing effect than the dark matter. Thus, at any given halo mass, the halos with less massive galaxies are much less likely to be strong lenses, resulting in a bias towards higher stellar mass fractions in strong lenses as compared to halos selected at random.

At the high mass end, one can directly identify clusters and groups corresponding to dark matter halos, and measure the stellar masses of their central galaxies. Yang et al. (2009a) use a group catalog matched to halos to determine halo masses (via an iteratively-computed group luminosity–mass relation). Stellar masses in this work are determined using the Bell et al. (2003) relation between $g - r$ color and M/L; a WMAP3 cosmology was assumed. Their results agree very well with ours for low-mass halos, but they begin to differ at higher masses. This may be partially due to scatter between their calculated halo masses (based on total stellar mass in the groups) and the true halo masses, resulting in additional scatter in their stellar masses at fixed halo mass. It could also be due to differences in stellar modeling; their results remain at all times within our systematic errors. We also compare to direct measurements of massive clusters by Hansen et al. (2009) and Lin & Mohr (2004). In order to convert luminosities to stellar masses, we assume $M/L_{i0.25} = 3.3 M_\odot/L_{\odot,i0.25}$ and M/L_K

$= 0.83 M_\odot/L_{\odot,K}$ based on the population synthesis code of Conroy et al. (2009). These measurements are both somewhat higher than our results for massive clusters, the one-sigma error estimates overlap. The discrepancies may be due to issues with cluster selection and with modeling scatter in the mass-observable relation; in each case the cluster mass is an average mass for the given observable (X-ray luminosity or cluster richness), and can result in a bias if central galaxies are correlated with this observable. More detailed modeling of the scatter and correlations will be required to determine whether this is can account for the offsets.

A comparison of our results to others at $z \sim 1$ is shown in Figure 12. As may be expected, it is much harder to directly measure the SM–HM relation at higher redshifts, resulting in relatively fewer published results with which we may compare. We first note that we have compared the impact of two independent measurements of the GSMF from different surveys. As discussed in 4.3.5, because we simultaneously fit our model with linear evolution to the GSMF at redshifts $0 < z < 1$, our results are less sensitive to sample variance. In contrast to the conclusion of Drory et al. (2009) which fit their results to specific redshift bins, Figure 12 shows that the Drory et al. (2009) and Pérez-González et al. (2008) results are in agreement within statistical errors at $z \sim 1$ when fitting the full redshift range. The results in Moster et al. (2009) are also very similar to ours at $z \sim 1$. However, Moster et al. (2009) do not give fits for the SM–HM relation which include the effects of scatter in stellar mass at fixed halo mass except at $z \sim 0$ and do not in general include scatter in measured stellar mass with respect to the true stellar mass. Hence, we include for comparison an SM–HM relation derived using our analysis but excluding both of these effects. The remaining deviance most likely stems from sample variance due to the much smaller survey volume on which their fit is based.

At $z \sim 1$, Wang & Jing (2009) make use of clustering data and stellar mass functions from the VVDS survey (Meneux et al. 2008; Pozzetti et al. 2007) at $z \sim 0.8$. At the same time, the high-mass and low-mass slopes of their power-law relation are not re-fit for the higher redshift, leading to similar deviations from our results as at $z \sim 0.1$. The results in Zheng et al. (2007) lie slightly below our results at $z \sim 1$. This is partially due to their use of a WMAP1 cosmology. However, it is difficult to say exactly how much, as their stellar masses at $z \sim 1$ are a hybrid of K_s-derived masses from Bundy et al. (2006) and color–based masses derived in a manner analogous to Bell et al. (2003). Nonetheless, they remain well within our systematic error bars.

We also include a comparison to the $z = 1$ SM–HM relation presented in Conroy & Wechsler (2009), who also use an abundance matching technique to assign galaxies to halos. Unique to the work of Conroy & Wechsler (2009) is their attempt to jointly fit both the redshift–dependent stellar mass functions and the redshift–dependent star formation rate – stellar mass relations. In their model, halo growth is tracked through time using results derived from halo merger trees, allowing galaxies to be identified across epochs. The evolution of halos in conjunction with standard abundance matching provides model predictions for star formation rates. The SM–HM relation from Conroy & Wechsler (2009) lies slightly above our best–fit relation, and it is within statistical error bars except at the very highest halo masses. This is due to the different assumptions made about the GSMF in the two works and also to the absence of corrections for the scatter in stellar mass at fixed halo mass in Conroy & Wechsler (2009).

Finally, the strong lensing survey of Gavazzi et al. (2007) has been extended by (Lagattuta et al. 2009) out to $z \sim 0.9$ using lenses observed in the CASTLES program, as well as in COSMOS and in the EGS. While the same caveats about selection effects apply as for lower redshifts, Lagattuta et al. (2009) find that the evolution in the stellar mass fraction for $M_h \sim 10^{13.5} M_\odot$ halos is within 0-0.3 dex greater at $z \sim 0.9$ as compared to $z \sim 0$, consistent with our limits of 0-0.15 dex for the allowed evolution over that redshift interval.

5. RESULTS BEYOND $z = 1$

5.1. *Methodology and Data Limitations*

As discussed in §2.1.2, published results for the galaxy stellar mass function beyond $z = 1$ suffer from the important caveat that integrated SFRs are inconsistent with galaxy stellar mass functions when both sets of observations are taken at face value with a constant IMF. Nonetheless, one may use similar methodology as in §3 to derive stellar mass – halo mass relations at higher redshifts under the assumption that the observed stellar mass functions are correct. Here we assume the GSMFs of Marchesini et al. (2009), which cover a redshift range of $1.3 < z < 4$.

As there is no guarantee that the evolution of the SM – HM relation at high redshifts will have the same form as its evolution at low redshifts, we re-examine the assumptions affecting our evolution parameterization in Equation 23. As with all current high-redshift data, the results in Marchesini et al. (2009) are limited to luminous (massive) galaxies, so little information about the value of β (the faint-end slope of the galaxy-halo mass relation) is available. Hence, we continue to assume a linear functional form for its evolution; as the value of β evolves linearly with scale factor (a) in our fit, this means that it is largely constrained to be consistent with the evolution at lower redshifts ($1 < z < 2$). Naturally, if the evolution of β at high redshifts is significantly different than for $1 < z < 2$, then our error bars for β may underestimate the full uncertainties in the parameter.

Additionally, the systematics affecting high-mass galaxies at high redshifts are much more severe than for $z < 1$. Not only are the errors in stellar mass calculations significant (due to larger photometry errors, limited templates, etc.), but any miscalibration in correcting photometric redshift errors will result in low-redshift galaxies masquerading as very bright high-redshift galaxies. These combined uncertainties result in poor constraints on high-mass galaxies. For that reason, we do not attempt to assume a more complicated functional form for the evolution of δ and γ, which means as before that their rates of evolution are largely constrained to be consistent with lower redshifts.

However, we find that individual fits at each redshift do suggest a possible evolution for the characteristic stellar mass which is nonlinear in the scale factor. Hence, we expand the form of the evolution of $M_{*,0}$ to include a quadratic dependence on scale factor:

$$M_{*,0}(a) = M_{*,0,0} + M_{*,0,a}(a-1) + M_{*,0,a^2}(a-0.5)^2, \quad (25)$$

where $(a-0.5)^2$ is used instead of $(a-1)^2$ to minimize the degeneracy between $M_{*,0,a}$ and $M_{*,0,a^2}$. We parameterize the evolution of all other parameters as in Equation 23. All other methodology remains the same as for lower redshifts, as outlined in §3.6.
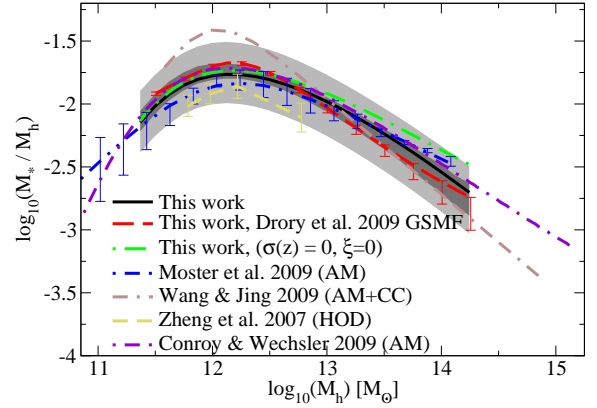
5.2. *Results*

Figure 12. Comparison of our best-fit model at $z = 1.0$ for different model assumptions and to previously published results. Dark grey shading indicates statistical and sample variance errors; light grey shading includes systematic errors. The error bars for the red line, calculated using the Drory et al. (2009) GSMF include statistical errors only—i.e., they do not include sample variance. The results of Moster et al. (2009) (green line) do not include modeling of scatter or statistical errors in stellar masses, so for comparison, we present our results excluding the effects of $\sigma(z)$ and ξ (blue line). The results of Conroy & Wechsler (2009) made slightly different assumptions about the stellar mass function evolution.

To maintain some overlap with the $z < 1$ results, we evaluate the likelihood function for each SM – HM relation against GSMFs for $0.8 < z < 4$. This data range includes two redshift bins from Pérez-González et al. (2008) (0.8-1.0, 1.0-1.3) and three redshift bins from Marchesini et al. (2009) (1.3-2, 2-3, 3-4). Including more redshift bins from Pérez-González et al. (2008) would improve the continuity of the fits to the low-redshift results; however, doing so would require a more complicated redshift parameterization than what we have assumed. The evolution of the best-fit stellar mass fraction for $0 < z < 4$ is shown in Figure 13. All data points for Figure 13 are listed in Appendix D.

As may be expected, uncertainties at high redshifts are substantially larger than at lower redshifts. The contribution of systematic errors in stellar masses to the error budget (0.25 dex) is still important, but it is no longer the only dominant factor. Statistical errors due to the comparatively small number of galaxy observations at high redshifts can contribute an equal uncertainty (up to 0.25 dex) to the derived SM–HM relation. The statistical errors are large not only for massive galaxies with low number counts, but also for halos below $10^{12} M_\odot$, where magnitude limits on surveys make observations of the corresponding galaxies difficult.

The contribution from other sources of uncertainties (e.g., sample variance, cosmology uncertainties) is substantially smaller than the current statistical errors. The effects of sample variance on uncertainties at high redshift is less than for low redshifts because the volume probed in the high redshift sample is five times larger than for the low redshift sample ($\approx 5 \times 10^6$ Mpc^3 vs. 10^6 Mpc^3, respectively). While cosmology uncertainties are somewhat larger at high redshifts, their contribution to the overall levels of uncertainty are again much smaller than the statistical errors, as was true even by $z = 1$ for the low-redshift sample.

The statistical uncertainties at high redshifts mean that it is difficult to draw strong conclusions about the evolution
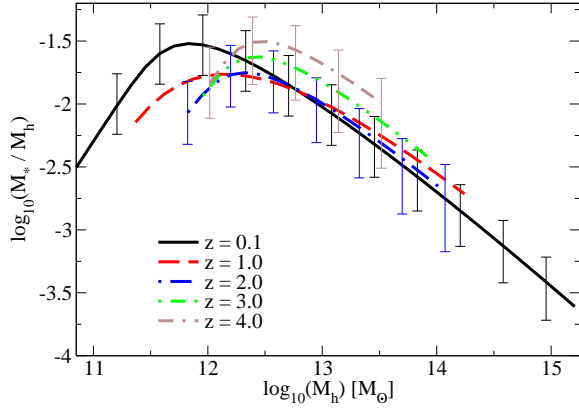
Figure 13. Evolution of the derived stellar mass fractions for central galaxies, from $z = 4$ to the present. The best–fit relations are shown only over the mass range where constraining data are available. At higher redshifts, certainty about the shape of the curves drops precipitously owing to a lack of constraining data beyond the knee of the stellar mass function. Combined systematic and statistical error bars are shown for three redshift bins only.

of the SM–HM relation. However, the indication is that the mass corresponding to the peak efficiency for star formation evolves slowly, and is roughly a factor of five larger at $z = 4$. At all redshifts, the integrated star formation peaks at ~ 10-20 per cent of the universal baryon fraction; the current data indicates that this value may start high at very high redshifts, shrink as halos grow faster than they form stars, and then start growing again after $z = 2$. However, with current uncertainties these results are tenuous. The single most effective way to reduce current uncertainties on both the SM–HM relation at individual redshifts and on its evolution is to conduct more high-redshift galaxy surveys, both to probe fainter galaxies to determin the shape of the GSMF and to get better statistics at the high mass end.

6. DISCUSSION AND IMPLICATIONS

At $z \sim 0$, the majority of published results are in accord within our full systematic error bars, regardless of the technique used. All reported results appear to be consistent with the principles necessary for abundance matching over a wide range of halo masses ($10^{11} - 10^{15} \, M_\odot$)—that each dark matter halo and subhalo above the masses we have considered hosts a galaxy with a reasonably tight relationship between their masses, and that average stellar mass — halo mass relation increases monotonically with halo mass.

Because of the available statistics of halo and galaxy stellar mass functions, especially at $z = 0$, the technique of abundance matching offers the tightest constraints on the SM–HM relation currently available, and it is in agreement with results from a broad variety of additional techniques. Under the assumption that systematic errors in stellar mass calculations do not change substantially with redshift, abundance matching offers tight constraints on the evolution of the SM–HM relation from $z = 1$ to the present. These in turn will serve as important new tests for star formation prescriptions and recipes in both hydrodynamical simulations and semi-analytic models, as they will apply on the level of individual halos instead of on the simulated volume as a whole.

At the same time, abundance matching offers these con-

straints with a minimal number of parameters. The Halo Occupation Distribution (HOD) technique requires modeling $P(N|M_h)$, the probability distribution of the number of galaxies per halo as a function of halo mass, in several different luminosity bins. In the model proposed in Zheng et al. (2007), this results in 45 fitted parameters just to models the occupation at $z = 0$ (five parameters for nine luminosity bins). Conditional Luminosity Function (CLF) modeling requires parameterizing a form for $\phi(L, M_h)$, the number density of galaxies as a function of luminosity and host halo mass, which results in approximately a dozen parameters to model occupation at $z = 0$ (Cooray 2006). Because of the additional constraints imposed by assuming that each halo hosts a galaxy, our approach uses fewer parameters. Abundance matching, as discussed in this paper, results in a model with only six independent parameters (five to empirically fit the derived SM–HM relation, and one to model the scatter in observed stellar masses at fixed halo mass) to describe the population of galaxies in halos.

The abundance matching approach to the SM–HM relation requires so few parameters in comparison to other methods because of the fairly small scatter (≈ 0.16 dex) between stellar mass and halo mass at high masses (the scatter has a negligible impact on the average SM–HM relation at lower masses), and the requirement that satellite galaxies live in satellite halos (subhalos). It may well be that a more complicated model must be adopted for satellites to quantitatively match the small-scale clustering observations (e.g. Wang et al. 2006). However, such changes will affect the clustering much more than the derived SM–HM relation, as suggested by the minimal changes in Figures 7 and 10 for mass scales ($\lesssim 10^{12.5}$ $M_\odot$) where satellites are a non-negligible fraction of the total halo population.

The largest uncertainties in the SM — HM relation at $z < 1$ come from assumptions in converting galaxy luminosities into stellar masses, which amount to uncertainties on the order of 0.25 dex in the normalization of the relation. However, the systematic biases introduced by the combined sources of scatter between calculated stellar masses and halo masses can rise to equivalent significance for halos above $10^{14.5} \, M_\odot$. Because the GSMF is monotonically decreasing, results which do not account for all sources of scatter in stellar mass will over-predict the average stellar mass in halos by 0.17-0.25 dex for these massive halos.

Using abundance matching to find confidence intervals for the SM–HM relation is an even more involved process, as each of the ways in which the systematics might vary must also be taken into account. While future work on constraining stellar masses will be the most valuable in terms of reducing uncertainties for the lowest redshift data, wider and deeper surveys and some resolution to the discrepancy between high-redshift cosmic star formation density and stellar mass functions must occur in order to improve constraints on the relation at high redshifts.

As mentioned in the introduction, abundance matching may be used equally well to assign galaxy luminosities and colors to halos. In this case, the galaxy luminosity — halo mass relation may be derived using identical methodology to that presented in §3, with the exception that the systematics μ and κ may be neglected, leaving only $\sigma(z)$ (effectively, the redshift scaling of photometry errors) and ξ (effectively, the scatter in luminosity at fixed halo mass). As these systematics are much better constrained than their stellar mass counterparts (simply as luminosities may be measured directly), this approach can

yield very powerful constraints on the normalization as well as the evolution of the luminosity–mass relation. The higher accuracy possible compared to the stellar mass–mass relation will generally *not* remove uncertainties in comparing to galaxy formation models. Galaxy formation codes which calculate luminosities must include modeling for all the effects in §2.1.1, meaning that constraints on the underlying physics are subject to the same uncertainties. However, tighter constraints on the luminosity–mass relation will be nonetheless helpful for applications which are concerned with cosmological constraints from large luminosity-selected surveys.

7. CONCLUSIONS

We have performed an extensive exploration of the uncertainties relevant to determining the relationship between dark matter halos and galaxy stellar masses from the halo abundance matching technique. Errors related to the observed stellar mass function, the theoretical halo mass function, and the underlying technique of abundance matching are all considered. We focus on the mean stellar mass to halo mass ratio for central galaxies as a function of halo mass, and present results for this relationship at the present epoch and extending to $z \sim 4$. We account separately for statistical errors and for systematic errors resulting from uncertainties in stellar mass estimation, and also investigate the relative contribution of various sources of error including cosmological uncertainty and the scatter between stellar mass and halo mass. An analytic model has been developed which can be used to constrain this connection in the absence of high resolution simulations.

Our primary conclusions are as follows:

1. The peak integrated star formation efficiency occurs at a halo mass near 10^{12} $M_\odot$, with a relatively low fraction — 20% at $z = 0$ — of baryons currently locked up in stars. This peak value declines to $z \sim 2$ but remains between 10–20% for all redshifts between $z = 0$–4. This implies that $30-40\%$ of baryons were converted into stars over the lifetime of a galaxy with current halo mass of 10^{12} $M_\odot$.

2. At low masses, the stellar mass – halo mass relation at $z = 0$ scales as $M_* \sim M_h^{2.3}$. At high masses, around 10^{14} $M_\odot$, stellar mass scales as $M_* \sim M_h^{0.29}$. However, the high mass scaling may not be a power law, as our model indicates that this slope decreases with increasing halo mass.

3. Within statistical uncertainties, the stellar mass content of halos has increased by $0.3 - 0.45$ dex for halos with mass less than 10^{12} $M_\odot$ since $z \sim 1$. Systematic biases in stellar mass calculations between different redshifts could broaden the uncertainties in this number, but the conclusion that significant evolution has occurred for low-mass halos would remain robust. For halos with mass greater than $10^{13}M_\odot$, our best-fit results indicate more growth in halo masses than stellar masses since $z \sim 1$, but are consistent with no evolution in the stellar mass fractions over this time.

4. Systematic, uniform offsets in the galaxy stellar mass function and its evolution are the dominant uncertainty in the stellar mass – halo mass relation at low redshift. Statistical errors in the estimation of individual stellar masses impact the high mass end of the GSMF, and at higher redshifts may result in an observed GSMF that deviates from a Schechter function.

5. Current uncertainties in the underlying cosmological model are sub-dominant to the systematic errors, but are larger than other sources of statistical error for halos below $M_h \sim 10^{12}$ $M_\odot$ for low redshifts ($z < 0.2$).

6. Given current constraints from other methods, uncertainty in the value of scatter between stellar mass and halo mass is important in the mean relation for masses above $M_h \sim 10^{12.5}$ $M_\odot$, although it is subdominant to systematic errors for all masses below $M_h \sim 10^{14.5}$ $M_\odot$.

7. Other uncertainties in the galaxy–halo assignment, including different assumptions about the treatment of satellite galaxies, are subdominant when considering the mean relation for central galaxies.

8. At higher redshifts ($1 < z < 4$), systematic uncertainties remain important, but statistical uncertainties reach equal significance. The shape of the relation is fairly unconstrained at $z > 2$, where improved statistics and constraints on the GSMF below $M*$ are needed.

We have presented a best–fit galaxy stellar mass – halo mass relation including an estimate of the total statistical and systematic errors using available data from $z = 0 - 4$, although caution should be used at redshifts higher than $z \sim 1$. We also present an algorithm to generalize this relation for an arbitrary cosmological model or halo mass function. The fact that assignment errors are sub-dominant and scatter can be well–constrained by other means gives increased confidence in using the simple abundance matching approach to constrain this relation. These results provide a powerful constraint on models of galaxy formation and evolution.

REFERENCES

Ashman, K. M., Salucci, P., & Persic, M. 1993, MNRAS, 260, 610

Baldry, I. K., Glazebrook, K., & Driver, S. P. 2008, MNRAS, 388, 945
Bell, E. F., McIntosh, D. H., Katz, N., & Weinberg, M. D. 2003, ApJ, 585, L117
Berlind, A. A., & Weinberg, D. H. 2002, ApJ, 575, 587
Berrier, J. C., Bullock, J. S., Barton, E. J., Guenther, H. D., Zentner, A. R., & Wechsler, R. H. 2006, ApJ, 652, 56
Blanton, M. R., & Roweis, S. 2007, AJ, 133, 734
Bruzual, G. 2007, arXiv:astro-ph/0703052
Bruzual, G., & Charlot, S. 2003, MNRAS, 344, 1000
Bryan, G. L., & Norman, M. L. 1998, ApJ, 495, 80
Bullock, J. S., Wechsler, R. H., & Somerville, R. S. 2002, MNRAS, 329, 246
Bundy, K., et al. 2006, ApJ, 651, 120
Calzetti, D., Armus, L., Bohlin, R. C., Kinney, A. L., Koornneef, J., & Storchi-Bergmann, T. 2000, ApJ, 533, 682
Cappellari, M., et al. 2006, MNRAS, 366, 1126
Cattaneo, A., Dekel, A., Faber, S. M., & Guiderdoni, B. 2008, MNRAS, 389, 567
Chabrier, G. 2003, Publications of the Astronomical Society of the Pacific, 115, 763
Charlot, S. 1996, in Astronomical Society of the Pacific Conference Series, Vol. 98, From Stars to Galaxies: the Impact of Stellar Physics on Galaxy Evolution, 275
Charlot, S., & Fall, S. M. 2000, ApJ, 539, 718
Charlot, S., Worthey, G., & Bressan, A. 1996, ApJ, 457, 625
Cole, S., et al. 2001, MNRAS, 326, 255
Colín, P., Klypin, A. A., Kravtsov, A. V., & Khokhlov, A. M. 1999, ApJ, 523, 32
Conroy, C., Gunn, J. E., & White, M. 2009, ApJ, 699, 486
Conroy, C., et al. 2007, ApJ, 654, 153
Conroy, C., & Wechsler, R. H. 2009, ApJ, 696, 620
Conroy, C., Wechsler, R. H., & Kravtsov, A. V. 2006, ApJ, 647, 201
Conroy, C., White, M., & Gunn, J. E. 2010, ApJ, 708, 58
Cooray, A. 2006, MNRAS, 365, 842
Cooray, A., & Sheth, R. 2002, Phys. Rep., 372, 1
Crocce, M., Fosalba, P., Castander, F. J., & Gaztanaga, E. 2009, arXiv:0907.0019 [astro-ph]
Davé, R. 2008, MNRAS, 385, 147
Dressler, A. 1980, ApJ, 236, 351
Driver, S. P., Popescu, C. C., Tuffs, R. J., Liske, J., Graham, A. W., Allen, P. D., & de Propris, R. 2007, MNRAS, 379, 1022
Drory, N., et al. 2009, arXiv:0910.5720 [astro-ph]
Dunkley, J., Bucher, M., Ferreira, P. G., Moodley, K., & Skordis, C. 2005, MNRAS, 356, 925
Eddington, Sir, A. S. 1940, MNRAS, 100, 354
Gavazzi, R., Treu, T., Rhodes, J. D., Koopmans, L. V. E., Bolton, A. S., Burles, S., Massey, R. J., & Moustakas, L. A. 2007, ApJ, 667, 176
Guo, Q., White, S., Li, C., & Boylan-Kolchin, M. 2009, arXiv:0909.4305 [astro-ph]
Guzik, J., & Seljak, U. 2002, MNRAS, 335, 311
Hansen, S. M., Sheldon, E. S., Wechsler, R. H., & Koester, B. P. 2009, ApJ, 699, 1333
Hilbert, S., White, S. D. M., Hartlap, J., & Schneider, P. 2007, MNRAS, 382, 121
Hopkins, A. M., & Beacom, J. F. 2006, ApJ, 651, 142
Hopkins, A. M., & Beacom, J. F. 2006, ApJ, 651, 142
Jenkins, A., et al. 2001, MNRAS, 321, 372
Kajisawa, M., et al. 2009, ApJ, 702, 1393
Kannappan, S. J., & Gawiser, E. 2007, ApJ, 657, L5
Kauffmann, G., et al. 2003, MNRAS, 341, 33
Kewley, L. J., Jansen, R. A., & Geller, M. J. 2005, PASP, 117, 227
Klypin, A., Gottlöber, S., Kravtsov, A. V., & Khokhlov, A. M. 1999, ApJ, 516, 530
Klypin, A., Trujillo-Gomez, S., & Primack, J. 2010, ArXiv e-prints
Klypin, A., et al. 2009, ApJ, in preparation
Komatsu, E., et al. 2009, ApJS, 180, 330
Kravtsov, A., & Klypin, A. 1999, ApJ, 520, 437
Kravtsov, A. V., Berlind, A. A., Wechsler, R. H., Klypin, A. A., Gottloeber, S., Allgood, B., & Primack, J. R. 2004, ApJ, 609, 35
Kravtsov, A. V., Gnedin, O. Y., & Klypin, A. A. 2004, ApJ, 609, 482
Kravtsov, A. V., Klypin, A. A., & Khokhlov, A. M. 1997, ApJ, 111, 73
Lagattuta, D. J., et al. 2009, arXiv:0911.2236 [astro-ph]
Le Borgne, D., Rocca-Volmerange, B., Prugniel, P., Lançon, A., Fioc, M., & Soubiran, C. 2004, A&A, 425, 881
Lee, H.-c., Worthey, G., Trager, S. C., & Faber, S. M. 2007, ApJ, 664, 215
Lee, S., Idzi, R., Ferguson, H. C., Somerville, R. S., Wiklind, T., & Giavalisco, M. 2009, ApJS, 184, 100
Leitherer, C., et al. 1999, ApJS, 123, 3
Li, C., Jing, Y. P., Kauffmann, G., Börner, G., Kang, X., & Wang, L. 2007, MNRAS, 376, 984

Li, C., & White, S. D. M. 2009, MNRAS, 398, 2177
Lin, Y.-T., & Mohr, J. J. 2004, ApJ, 617, 879
Lucatello, S., Gratton, R. G., Beers, T. C., & Carretta, E. 2005, ApJ, 625, 833
Mandelbaum, R., Seljak, U., Kauffmann, G., Hirata, C. M., & Brinkmann, J. 2006, MNRAS, 368, 715
Maraston, C. 2005, MNRAS, 362, 799
Marchesini, D., van Dokkum, P. G., Förster Schreiber, N. M., Franx, M., Labbé, I., & Wuyts, S. 2009, ApJ, 701, 1765
Marín, F. A., Wechsler, R. H., Frieman, J. A., & Nichol, R. C. 2008, ApJ, 672, 849
Meneux, B., et al. 2008, A&A, 478, 299
—. 2009, A&A, 505, 463
More, S., van den Bosch, F. C., Cacciato, M., Mo, H. J., Yang, X., & Li, R. 2009, MNRAS, 392, 801
Moster, B. P., Somerville, R. S., Maulbetsch, C., van den Bosch, F. C., Maccio', A. V., Naab, T., & Oser, L. 2009, arXiv:0903.4682 [astro-ph]
Muzzin, A., Marchesini, D., van Dokkum, P. G., Labbé, I., Kriek, M., & Franx, M. 2009, ApJ, 701, 1839
Nagai, D., & Kravtsov, A. V. 2005, ApJ, 618, 557
Nagamine, K., Ostriker, J. P., Fukugita, M., & Cen, R. 2006, The Astrophysical Journal, 653, 881
Nagamine, K., Ostriker, J. P., Fukugita, M., & Cen, R. 2006, ApJ, 653, 881
Neyrinck, M. C., Hamilton, A. J. S., & Gnedin, N. Y. 2004, MNRAS, 348, 1
Panter, B., Heavens, A., & Jimenez, R. 2004, MNRAS, 355, 764
Panter, B., Jimenez, R., Heavens, A. F., & Charlot, S. 2007, MNRAS, 488
Percival, S. M., & Salaris, M. 2009, ApJ, 703, 1123
Pérez-González, P. G., et al. 2005, ApJ, 630, 82
—. 2008, ApJ, 675, 234
Postman, M., & Geller, M. J. 1984, ApJ, 281, 95
Pozzetti, L., et al. 2007, A&A, 474, 443
Prada, F., et al. 2003, ApJ, 598, 260
Press, W. H., & Schechter, P. 1974, ApJ, 187, 425
Reddy, N. A., & Steidel, C. C. 2009, ApJ, 692, 778
Salimbeni, S., Fontana, A., Giallongo, E., Grazian, A., Menci, N., Pentericci, L., & Santini, P. 2009, in American Institute of Physics Conference Series, Vol. 1111, American Institute of Physics Conference Series, ed. G. Giobbi, A. Tornambe, G. Raimondo, M. Limongi, L. A. Antonelli, N. Menci, & E. Brocato, 207–211
Salpeter, E. E. 1955, ApJ, 121, 161
Shankar, F., Lapi, A., Salucci, P., De Zotti, G., & Danese, L. 2006, ApJ, 643, 14
Sheldon, E. S., et al. 2004, AJ, 127, 2544
Spergel, D. N., et al. 2003, ApJS, 148, 175
Springel, V. 2005, MNRAS, 364, 1105
Stanek, R., Rudd, D., & Evrard, A. E. 2009, MNRAS, 394, L11
Tasitsiomi, A., Kravtsov, A. V., Wechsler, R. H., & Primack, J. R. 2004, ApJ, 614, 533
Tinker, J., Kravtsov, A. V., Klypin, A., Abazajian, K., Warren, M., Yepes, G., Gottlöber, S., & Holz, D. E. 2008, ApJ, 688, 709
Tinker, J. L., Weinberg, D. H., Zheng, Z., & Zehavi, I. 2005, ApJ, 631, 41
Tinsley, B. M., & Gunn, J. E. 1976, ApJ, 203, 52
Tumlinson, J. 2007a, ApJ, 665, 1361
—. 2007b, ApJ, 664, L63
Vale, A., & Ostriker, J. P. 2004, MNRAS, 353, 189
—. 2006, MNRAS, 371, 1173
van den Bosch, F. C., Norberg, P., Mo, H. J., & Yang, X. 2004, MNRAS, 352, 1302
van der Wel, A., Franx, M., Wuyts, S., van Dokkum, P. G., Huang, J., Rix, H.-W., & Illingworth, G. D. 2006, ApJ, 652, 97
van Dokkum, P. G. 2008, ApJ, 674, 29
Wang, L., & Jing, Y. P. 2009, arXiv:0911.1864 [astro-ph]
Wang, L., Li, C., Kauffmann, G., & de Lucia, G. 2006, MNRAS, 371, 537
Warren, M. S., Abazajian, K., Holz, D. E., & Teodoro, L. 2006, ApJ, 646, 881
Weinberg, D. H., Colombi, S., Davé, R., & Katz, N. 2008, ApJ, 678, 6
Weinberg, D. H., Davé, R., Katz, N., & Hernquist, L. 2004, ApJ, 601, 1
Wetzel, A. R., & White, M. 2009, arXiv:0907.0702 [astro-ph]
Wilkins, S. M., Trentham, N., & Hopkins, A. M. 2008a, MNRAS, 385, 687
—. 2008b, MNRAS, 385, 687
Yang, X., Mo, H. J., & van den Bosch, F. C. 2009a, ApJ, 695, 900
—. 2009b, ApJ, 693, 830
Yang, X., Mo, H. J., van den Bosch, F. C., Pasquali, A., Li, C., & Barden, M. 2007, ApJ, 671, 153
Yang, X., et al. 2003, MNRAS, 339, 1057
Yi, S. K. 2003, ApJ, 582, 202
York, D. G., et al. 2000, AJ, 120, 1579
Zaritsky, D., & White, S. D. M. 1994, ApJ, 435, 599
Zheng, Z., Coil, A. L., & Zehavi, I. 2007, ApJ, 667, 760

APPENDIX

CONVERTING RESULTS TO OTHER HALO MASS FUNCTIONS

From Equation 14, it is possible to simply convert from our halo mass function ϕ_h to any halo mass function of choice ($\phi_{h,r}$). In particular, the function $M_h(M_*)$ is defined by the fact that the number density of halos with mass above $M_h(M_*)$ must match the number density of galaxies with stellar mass above M_* (with the appropriate deconvolution steps applied). Recall from Equation 14 that

$$\int_{M_h(M_*)}^{\infty} \phi_h(M) d\log_{10} M = \int_{M_*}^{\infty} \phi_{\text{direct}}(M_*) d\log_{10} M_*. \tag{A1}$$

Naturally, the correct mass-stellar mass relation for the alternate halo mass function $\phi_{h,r}$ (which we will label as $M_{h,r}(M_*)$) must satisfy this same equation, with the result that:

$$\int_{M_h(M_*)}^{\infty} \phi_h(M) d\log_{10} M = \int_{M_{h,r}(M_*)}^{\infty} \phi_{h,r}(M) d\log_{10} M. \tag{A2}$$

To make the calculation even more explicit, let $\Phi_h(M) = \int_M^{\infty} \phi_h d\log_{10} M$ be our cumulative halo mass function, and let $\Phi_{h,r}(M)$ be the corresponding cumulative halo mass function for $\phi_{h,r}$. Then, we find:

$$M_{h,r}(M_*) = \Phi_{h,r}^{-1}(\Phi_h(M_h(M_*))). \tag{A3}$$

Mass functions from different cosmologies than those assumed in this paper will also require converting stellar masses if their choices of h differ from the WMAP5 best-fit value.

EFFECTS OF SCATTER ON THE STELLAR MASS FUNCTION

This section is intended to provide basic intuition for the effects of both ξ and $\sigma(z)$, which may be modeled as convolutions. The classic example in this case is convolution of the GSMF with a log-normal distribution of some width ω. While the convolution (even of a Schechter function) with a Gaussian has no known analytical solution, we may approximate the result by considering the case where the logarithmic slope of the GSMF changes very little over the width of the Gaussian. Then, locally, the stellar mass function is proportional to a power function, say $\phi(M_*) \propto (M_*)^\alpha$. Then, if we let $x = \log_{10} M_*$ (so that $\phi(10^x) \propto 10^{\alpha x}$), finding the convolution is equivalent to calculating the following integral:

$$\phi_{\text{conv}}(10^x) \propto \int_{-\infty}^{\infty} \frac{10^{\alpha b}}{\sqrt{2\pi\omega^2}} \exp\left(-\frac{(x-b)^2}{2\omega^2}\right) db$$
$$= 10^{\alpha x} 10^{\frac{1}{2}\alpha^2 \omega^2 \ln(10)}. \tag{B1}$$

That is to say, the stellar mass function is shifted upward by approximately $1.15 (\alpha\omega)^2$ dex. Hence, for parts of the stellar mass function with shallow slopes, the shift is completely insignificant, as it is proportional to α^2. However, it matters much more in the steeper part of the stellar mass function, to the point that for galaxies of mass $10^{12} M_\odot$, the observed stellar mass function can be several orders of magnitude above the intrinsic GSMF.

A SAMPLE CALCULATION OF THE FUNCTIONAL FORM OF THE STELLAR MASS FUNCTION

Galaxy formation models typically assume at least two feedback mechanisms to limit star formation for low-mass galaxies and for high-mass galaxies. Thus, one of the simplest fiducial star formation rate (SFR) as a function of halo mass (M_h) would assume a double power-law form:

$$SFR(M_h) \propto \left(\frac{M_h}{M_0}\right)^a + \left(\frac{M_h}{M_0}\right)^b. \tag{C1}$$

We might expect the total stellar mass as a function of halo mass to take a similar form, except perhaps with a wider region of transition between galaxies whose histories are predominantly low mass, and those with histories which are predominantly high mass, for the reason that some galaxies' accretion histories may have caused them to be affected comparably by both feedback mechanisms.

Hence, assuming that the relation between halo mass and stellar mass follows a double power-law form, we adopt a simple functional form to convert from the stellar mass of a galaxy to the halo mass:

$$M_h(M_*) = M_1 \left[\left(\frac{M_*}{M_{*,0}}\right)^{\beta/\gamma} + \left(\frac{M_*}{M_{*,0}}\right)^{\delta/\gamma} \right]^\gamma. \tag{C2}$$

Here, β may be thought of as the faint-end slope, δ as the massive-end slope (although β and δ are functionally interchangeable), and γ as the transition width (larger γ means a slower transition between the massive and faint-end slopes).

We first calculate $\frac{d\log(M_h)}{d\log(M_*)}$:

$$\log(M_h) = \log(M_1) + \gamma \log\left[\left(\frac{M_*}{M_{*,0}}\right)^{\beta/\gamma} + \left(\frac{M_*}{M_{*,0}}\right)^{\delta/\gamma} \right], \tag{C3}$$

$$\frac{d\log(M_h)}{d\log(M_*)} = \frac{d\log(M_h)}{dM_*} \frac{dM_*}{d\log(M_*)} \tag{C4}$$

$$= M_* \ln(10) \frac{d\log(M_h)}{dM_*} \tag{C5}$$

$$= \frac{\beta \left(\frac{M_*}{M_{*,0}}\right)^{\beta/\gamma} + \delta \left(\frac{M_*}{M_{*,0}}\right)^{\delta/\gamma}}{\left(\frac{M_*}{M_{*,0}}\right)^{\beta/\gamma} + \left(\frac{M_*}{M_{*,0}}\right)^{\delta/\gamma}} \tag{C6}$$

$$= \beta + (\delta - \beta) \left(1 + \left(\frac{M_*}{M_{*,0}}\right)^{\frac{\beta-\delta}{\gamma}}\right)^{-1}. \tag{C7}$$

This justifies the earlier intuition that the functional form for $M_h(M_*)$ transitions between slopes of β and δ with a width that increases with γ. Note that $\frac{d\log(M_h)}{d\log(M_*)}$ is always of order one, as the stellar mass is always assumed to increase with the halo mass and vice versa (namely, $\beta > 0$ and $\delta > 0$).

Next, we approach $\frac{dN}{d\log M_h}$. From analytical results, we expect a Schechter function for the halo mass function, namely:

$$\frac{dN}{d\log(M_h)} = \phi_0 \ln(10) \left(\frac{M_h}{M_0}\right)^{1-\alpha} \exp\left(-\frac{M_h}{M_0}\right). \tag{C8}$$

Substituting in the equation for $M_h(M_*)$, we have

$$\frac{dN}{d\log(M_h)} = \phi_0 \ln(10) \left[\left(\frac{M_*}{M_{*,0}}\right)^{\beta/\gamma} + \left(\frac{M_*}{M_{*,0}}\right)^{\delta/\gamma} \right]^{\gamma(1-\alpha)}$$
$$\times \left(\frac{M_h}{M_0}\right)^{1-\alpha} \exp\left(-\frac{M_1}{M_0}\left[\left(\frac{M_*}{M_{*,0}}\right)^{\beta/\gamma} + \left(\frac{M_*}{M_{*,0}}\right)^{\delta/\gamma}\right]^{\gamma}\right). \tag{C9}$$

Already evident is the generic result that there will be separate faint-end and massive-end slopes in the stellar mass function, and that the falloff is not generically specified by an exponential. We may make one simplification in this model—namely, to note that $M_h(M_{*,0})$ corresponds to the halo mass at which the slope of $M_h(M_*)$ begins to transition from β to δ. We expect this transition to correspond to the transition between supernova feedback and AGN feedback in semi-analytic models—namely, for a halo mass which is too large to be affected much by supernova feedback, but which is yet too small to host a large AGN. This implies that $M_h(M_{*,0})$ is expected to be around $10^{12}\ M_\odot$ or less, meaning that M_h/M_0 is small until stellar masses well beyond $M_{*,0}$, meaning that we may neglect the faint-end slope of the $M_h(M_*)$ relation in the exponential portion of the stellar mass function:

$$\frac{dN}{d\log(M_h)} = \phi_0 \ln(10) \left(\frac{M_1}{M_0}\right)^{1-\alpha} \left[\left(\frac{M_*}{M_{*,0}}\right)^{\beta/\gamma} + \left(\frac{M_*}{M_{*,0}}\right)^{\delta/\gamma} \right]^{\gamma(1-\alpha)}$$
$$\times \exp\left(-\frac{M_1}{M_0}\left(\frac{M_*}{M_{*,0}}\right)^{\delta}\right). \tag{C10}$$

Hence, we may combine these two equations to obtain the expression for the stellar mass function:

$$\frac{dN}{d\log(M_*)} = \phi_0 \ln(10) \left(\frac{M_1}{M_0}\right)^{1-\alpha} \left[\left(\frac{M_*}{M_{*,0}}\right)^{\beta/\gamma} + \left(\frac{M_*}{M_{*,0}}\right)^{\delta/\gamma} \right]^{\gamma(1-\alpha)}$$
$$\times \exp\left(-\frac{M_1}{M_0}\left(\frac{M_*}{M_{*,0}}\right)^{\delta}\right)$$
$$\times \left[\beta + (\delta - \beta)\left(1 + \left(\frac{M_*}{M_{*,0}}\right)^{\frac{\beta-\delta}{\gamma}}\right)^{-1}\right]. \tag{C11}$$

While this seems complicated, it may be intuitively deconstructed as:

$$\frac{dN}{d\log(M_*)} = [\text{constant}]\left[\text{double power law}\right]$$

$$\times \left[\text{exponential dropoff}\right]\mathcal{O}(1). \qquad (C12)$$

As mentioned previously, this functional form is equivalent to ϕ_{direct}. To convert to the true stellar mass function ϕ_{true} or the observed stellar mass function ϕ_{meas}, it must be convolved with the scatter in stellar mass at fixed halo mass and (for ϕ_{meas}) the scatter in calculated stellar mass at fixed true stellar mass. As such, it should be clear that—while the final form may be Schechter–*like*—there is certainly much more flexibility in the final shape of the GSMF than a Schechter function alone would allow, as evidenced by the five parameters required to fully specify equation C11.

DATA TABLES

We reproduce here listings of the data points in Figures 5, 6, and 13 in Tables 3, 4, and 5, respectively. See sections 4.2 and 5.2 for details on the data points in each table.

Table 3
Stellar Mass Fractions For $0 < z < 1$ Including Full Systematics

	$z = 0.1$	$z = 0.5$	$z = 1.0$
$\log_{10}(M_h)$	$\log_{10}(M_*/M_h)$	$\log_{10}(M_*/M_h)$	$\log_{10}(M_*/M_h)$
11.00	$-2.30^{+0.26}_{-0.23}$		
11.25	$-1.96^{+0.25}_{-0.23}$	$-2.11^{+0.22}_{-0.26}$	
11.50	$-1.67^{+0.24}_{-0.24}$	$-1.84^{+0.22}_{-0.26}$	$-2.01^{+0.25}_{-0.24}$
11.75	$-1.53^{+0.23}_{-0.24}$	$-1.70^{+0.24}_{-0.24}$	$-1.85^{+0.26}_{-0.23}$
12.00	$-1.54^{+0.24}_{-0.24}$	$-1.68^{+0.26}_{-0.23}$	$-1.77^{+0.26}_{-0.23}$
12.25	$-1.62^{+0.24}_{-0.24}$	$-1.72^{+0.26}_{-0.23}$	$-1.77^{+0.25}_{-0.23}$
12.50	$-1.74^{+0.24}_{-0.24}$	$-1.81^{+0.25}_{-0.23}$	$-1.81^{+0.24}_{-0.24}$
12.75	$-1.87^{+0.23}_{-0.25}$	$-1.92^{+0.25}_{-0.23}$	$-1.89^{+0.23}_{-0.26}$
13.00	$-2.02^{+0.23}_{-0.25}$	$-2.05^{+0.24}_{-0.24}$	$-1.99^{+0.22}_{-0.27}$
13.25	$-2.18^{+0.22}_{-0.26}$	$-2.19^{+0.24}_{-0.25}$	$-2.11^{+0.21}_{-0.28}$
13.50	$-2.35^{+0.22}_{-0.26}$	$-2.34^{+0.23}_{-0.25}$	$-2.25^{+0.21}_{-0.29}$
13.75	$-2.52^{+0.22}_{-0.27}$	$-2.51^{+0.23}_{-0.26}$	$-2.39^{+0.21}_{-0.30}$
14.00	$-2.70^{+0.21}_{-0.28}$	$-2.68^{+0.23}_{-0.26}$	$-2.55^{+0.22}_{-0.30}$
14.25	$-2.88^{+0.21}_{-0.28}$	$-2.86^{+0.23}_{-0.26}$	
14.50	$-3.07^{+0.20}_{-0.29}$	$-3.04^{+0.23}_{-0.27}$	
14.75	$-3.26^{+0.20}_{-0.30}$		
15.00	$-3.45^{+0.20}_{-0.30}$		

Note. — Halo masses are in units of $M_\odot$. Constraints are quoted over the mass range probed by the observed GSMF.

Table 4
Stellar Mass Fractions without Systematic Errors ($\mu = \kappa = 0$)

$\log_{10}(M_h)$	$z = 0.1$ $\log_{10}(M_*/M_h)$	$z = 0.5$ $\log_{10}(M_*/M_h)$	$z = 1.0$ $\log_{10}(M_*/M_h)$
11.00	$-2.30^{+0.03}_{-0.02}$		
11.25	$-1.96^{+0.04}_{-0.01}$	$-2.10^{+0.04}_{-0.08}$	
11.50	$-1.67^{+0.03}_{-0.01}$	$-1.83^{+0.05}_{-0.06}$	$-2.02^{+0.10}_{-0.06}$
11.75	$-1.53^{+0.01}_{-0.01}$	$-1.71^{+0.06}_{-0.03}$	$-1.85^{+0.10}_{-0.04}$
12.00	$-1.54^{+0.01}_{-0.02}$	$-1.68^{+0.06}_{-0.02}$	$-1.78^{+0.09}_{-0.03}$
12.25	$-1.62^{+0.00}_{-0.02}$	$-1.72^{+0.06}_{-0.01}$	$-1.77^{+0.08}_{-0.03}$
12.50	$-1.74^{+0.01}_{-0.02}$	$-1.81^{+0.05}_{-0.02}$	$-1.81^{+0.06}_{-0.04}$
12.75	$-1.87^{+0.01}_{-0.03}$	$-1.92^{+0.05}_{-0.02}$	$-1.88^{+0.04}_{-0.06}$
13.00	$-2.02^{+0.01}_{-0.03}$	$-2.05^{+0.04}_{-0.03}$	$-1.98^{+0.03}_{-0.08}$
13.25	$-2.18^{+0.02}_{-0.04}$	$-2.19^{+0.04}_{-0.04}$	$-2.10^{+0.04}_{-0.10}$
13.50	$-2.35^{+0.02}_{-0.05}$	$-2.34^{+0.04}_{-0.05}$	$-2.24^{+0.04}_{-0.13}$
13.75	$-2.52^{+0.03}_{-0.06}$	$-2.51^{+0.05}_{-0.06}$	$-2.38^{+0.05}_{-0.15}$
14.00	$-2.70^{+0.03}_{-0.07}$	$-2.68^{+0.05}_{-0.07}$	$-2.54^{+0.06}_{-0.17}$
14.25	$-2.88^{+0.04}_{-0.08}$	$-2.85^{+0.06}_{-0.08}$	
14.50	$-3.07^{+0.04}_{-0.09}$	$-3.04^{+0.06}_{-0.10}$	
14.75	$-3.25^{+0.05}_{-0.10}$		
15.00	$-3.45^{+0.05}_{-0.11}$		

Note. — Halo masses are in units of $M_\odot$.

Table 5
Stellar Mass Fractions For $0.8 < z < 4$ Including Full Systematics

$\log_{10}(M_h)$	$z = 1.0$ $\log_{10}(M_*/M_h)$	$z = 2.0$ $\log_{10}(M_*/M_h)$	$z = 3.0$ $\log_{10}(M_*/M_h)$	$z = 4.0$ $\log_{10}(M_*/M_h)$
11.50	$-2.01^{+0.25}_{-0.24}$			
11.75	$-1.85^{+0.26}_{-0.23}$			
12.00	$-1.77^{+0.26}_{-0.23}$	$-1.89^{+0.22}_{-0.27}$	$-1.89^{+0.25}_{-0.27}$	
12.25	$-1.77^{+0.25}_{-0.23}$	$-1.76^{+0.24}_{-0.25}$	$-1.67^{+0.21}_{-0.29}$	$-1.58^{+0.22}_{-0.32}$
12.50	$-1.81^{+0.24}_{-0.24}$	$-1.78^{+0.23}_{-0.26}$	$-1.63^{+0.21}_{-0.30}$	$-1.50^{+0.20}_{-0.35}$
12.75	$-1.89^{+0.23}_{-0.26}$	$-1.87^{+0.20}_{-0.30}$	$-1.71^{+0.19}_{-0.35}$	$-1.56^{+0.19}_{-0.40}$
13.00	$-1.99^{+0.22}_{-0.27}$	$-2.00^{+0.17}_{-0.35}$	$-1.83^{+0.17}_{-0.39}$	$-1.68^{+0.19}_{-0.44}$
13.25	$-2.11^{+0.21}_{-0.28}$	$-2.14^{+0.15}_{-0.39}$	$-1.97^{+0.16}_{-0.44}$	$-1.82^{+0.19}_{-0.49}$
13.50	$-2.25^{+0.21}_{-0.29}$	$-2.30^{+0.15}_{-0.42}$	$-2.13^{+0.17}_{-0.47}$	$-1.98^{+0.19}_{-0.52}$
13.75	$-2.39^{+0.21}_{-0.30}$	$-2.47^{+0.17}_{-0.45}$	$-2.30^{+0.19}_{-0.49}$	
14.00	$-2.55^{+0.22}_{-0.30}$	$-2.64^{+0.20}_{-0.47}$		

Note. — Halo masses are in units of $M_\odot$.